Spring 2018

It's not you, it's me: corollary discharge in the precerebellar nuclei of sleeping infant rats

Didhiti Mukherjee
University of Iowa

IT'S NOT YOU, IT'S ME: COROLLARY DISCHARGE IN THE PRECEREBELLAR NUCLEI OF SLEEPING INFANT RATS

by

Didhiti Mukherjee

A thesis submitted in partial fulfillment
of the requirements for the Doctor of Philosophy
degree in Psychology in the
Graduate College of
The University of Iowa

May 2018

Thesis Supervisor: Professor Mark S. Blumberg

Graduate College
The University of Iowa
Iowa City, Iowa

CERTIFICATE OF APPROVAL

_____

PH.D. THESIS

_____

This is to certify that the Ph.D. thesis of

Didhiti Mukherjee

has been approved by the Examining Committee for
the thesis requirement for the Doctor of Philosophy degree
in Psychology at the May 2018 graduation.

Thesis Committee: _____
Mark S. Blumberg, Thesis Supervisor

_____
Alan K. Johnson

_____
Eliot Hazeltine

_____
Ryan T. LaLumiere

_____
Jason J. Radley

Dedicated to:

My rat pups,
who made this dissertation possible

ACKNOWLEDGMENTS

I hereby express my sincere gratitude to all those people without whom this dissertation would never have been possible.

It was an honor to be a part of the Blumberg lab at the University of Iowa and to work and grow under the supervision of Professor Mark Blumberg. His expertise, constant support, and genuine care have nurtured my professional development and have left an indelible impression on my path in science. I thank him for being an incredible mentor and having faith in me.

I fall short of words to thank Dr. Greta Sokoloff who has been my pillar of support in the lab. I acquired scientific knowledge, techniques, and skills from her over the years. Moreover, her constant enthusiasm and inspiration never allowed me to succumb to unfavorable situations.

A special note of thanks to Carlos Del Rio-Bermudez, one of my fellow graduate students in the lab. Working together with him in the lab provided me with zeal and enthusiasm. Our endless discussions and exchange of thoughts have always been helpful for being productive and making science fun. I also thank him for being an outstanding friend and always having my back.

My heartfelt thanks to Dr. Alex Tiriac, a former graduate student in the lab, for everything. Not only he is one of the best teachers I have ever met, he is also a great example of a budding scientist. He has and will always be an inspiration for me in my scientific endeavors.

I thank Dr. Jimmy Dooley, Cassie Coleman, Lex Gomez, Ryan Glanz, Nick Sattler, Alex Fanning, Alex Yonk, Kev You, Rikki Laser and all other members of

the Blumberg lab for their moral support, technical assistance, and also for making the lab atmosphere really friendly and homey.

I also thank my dissertation committee members: Dr. Alan Kim Johnson, Dr. Ryan LaLumiere, Dr. Eliot Hazeltine, and Dr. Jason Radley for their guidance, advice, and suggestions.

Finally, it is time to thank my parents and my husband Abhisek, without whom nothing would have been possible. Despite being thousands of miles away, they have been behind me, beside me and with me always. Their unconditional love, constant support, and encouragement have helped me stay focused and overcome hurdles. I sincerely thank them for believing in me and supporting me in pursuing my dreams.

ABSTRACT

Developing animals primarily receive two kinds of somatosensory input. One arises from stimulation in the external environment ("exafference") and the other arises from self-produced movements ("reafference"), especially those associated with the myoclonic twitches during active sleep. Neural recordings have shown that exafferent and reafferent neural signals activate sensorimotor structures throughout the brain, but it is not known whether twitches are accompanied by corollary discharge that inform the nervous system that twitches are self-generated.

Recordings from the cerebellum in infant rats suggested that motor structures could be conveying twitch-related corollary discharge signals to the cerebellum. If true, one would expect to see evidence of corollary discharge in the precerebellar nuclei. We hypothesized that two precerebellar nuclei: the inferior olive (IO) and the lateral reticular nucleus (LRN), receive corollary discharge associated with the production of twitches. We tested the hypothesis by recording spontaneous activity of the IO and LRN during sleep and wake in infant rats.

In the majority of IO units, and in a subset of LRN units, neural activity was particularly pronounced at the time of twitch onset. This activity was remarkably precise, reaching a peak in firing within ±10 ms of a twitch. This unique pattern suggested that, unlike sensory areas that receive reafference from twitches, these two structures receive corollary discharge associated with the production of twitches.

Next, using anatomical tracing, immunohistochemistry, and neurophysiology, we identified non-overlapping premotor areas in the midbrain that send corollary discharge to the IO and LRN. Finally, using pharmacological inhibition, we identified that slow potassium channels are responsible for the sharp peak of twitch-related corollary discharge in the IO.

Altogether, the current findings suggest that the infant brain has the capacity to distinguish between exafferent stimulation and twitch-related reafference. This capacity may underlie the developing infant's burgeoning ability to distinguish between self- and other-generated movements.

PUBLIC ABSTRACT

Why can't we tickle ourselves? When we are tickled by someone else, it is "unexpected" and carries some level of surprise. In contrast, self-tickling is "expected" and we cannot, by definition, surprise ourselves. As a result, sensations arising from self-tickling is suppressed. This suggests that there is a mechanism that informs the nervous system whether a movement is self-generated and distinguishes it from movements that are other-generated.

Self-generated movements are not restricted to periods of wakefulness, especially during development. Infants move a lot when they are asleep. The brief, discrete movements during sleep are called myoclonic twitches and they are a predominant form of motor behavior during development. Interestingly, whereas sensations arising from self-generated wake movements are suppressed in certain brain structures, those arising from twitches are not. Accordingly, it has been proposed that twitches are processed in those structures *as if* they are other-generated, and hence unexpected.

In contrast, here we identify other brain structures in infant rats that process twitch-related information as if they are expected. This information originates from motor structures that are involved in twitch production and is conveyed to downstream structures to trigger activity. This activity exhibits unique signature features in relation to twitches; it is remarkably sharp, reaching a peak in firing at the onset of twitches. These features suggest that these structures receive the information that twitches are self-generated, and hence expected. We also

identified a cellular mechanism responsible for producing the sharp twitch-related peak.

Altogether, our results suggest that twitches help to instruct the developing brain to distinguish between self- and other-generated movements. Therefore, disruption of sleep during early development may have later-emerging negative consequences as observed in a number of neurodevelopmental disorders, including autism, and schizophrenia.

TABLE OF CONTENTS

LIST OF FIGURES

LIST OF ABBREVIATIONS

AS	active wake
AW	active sleep
bVFRT	bilateral ventral flexor reflex tract
C	cervical
DAO	dorsal accessory olive
DCN	deep cerebellar nuclei
Dk	nucleus Darkschewitsch
ECN	external cuneate nucleus
EMG	electromyography
EPSP	excitatory postsynaptic potential
GABA	gamma amino butyric acid
iFT	ipsilateral forelimb tract
IO	inferior olive
IP	intraperitoneal
IPSP	inhibitory postsynaptic potential
LRN	lateral reticular nucleus
MA3	accessory oculomotor nuclei
MAO	medial accessory olive
MDJ	mesodiencephalic junction
MUA	multiunit activity
P	postnatal day
PO	principal olive
BQ	behavioral quiescence
REM	rapid eye movement
RI	rostral interstitial nucleus of Cajal
RN	red nucleus
SK	calcium-activated slow potassium
WGA	wheat germ agglutinin

CHAPTER 1

Introduction

The sensorimotor system of vertebrate and invertebrate species responds to stimuli from the external environment (i.e., exafference) and to stimuli generated as a result of the animal's own behavior (i.e., reafference; Cullen, 2004). Sensory receptors are indifferent to the source of their activation. Therefore, in principle, they convey both "exafference" and "reafference" signals with equal efficiency (Crapse and Sommer, 2008). This could lead to potential problems in sensory processing because this will introduce ambiguity about the source of sensory input. In short, animals must be able to distinguish between sensory feedback arising from self-generated and other-generated movements.

To make this distinction, motor areas generate copies of motor commands, known as corollary discharge (CD; see Fig 1; Poulet and Hedwig, 2007; Crapse and Sommer, 2008), a term coined by Roger Sperry in the mid-nineteenth century (Sperry, 1950). Whereas a motor command is conveyed to the muscles to produce a movement, a CD is transmitted to non-motor, usually sensory areas, where it provides a "heads up" that the movement is self-generated and, therefore, predicted (Sommer and Wurtz, 2002). Subsequently, CD gates reafference resulting from the predicted movement. Gating of predicted reafference in sensory areas enhances the salience of unpredicted reafference, and thus, enables the animal to distinguish between "self-generated" and "other-generated" movements

(Poulet and Hedwig, 2007). The first experimental evidence of CD was presented in two studies by Sperry (1950) and von Holst and Mittelstaedt (1950).

Implications of corollary discharge across species

CD is necessary for proper functioning of nearly all sensory systems and is present in multiple levels of the nervous system in a diverse array of species (for review see Crapse and Sommer, 2008). For example, gastropods (e.g., *Pleurobranchaea*) exhibit a withdrawal response when unexpected contact is made with the tactile mechanoreceptors in their oral veil (i.e., mouth). Similarly, when they are feeding, they experience a substantial amount of tactile stimulation in their oral veil; nonetheless, the same withdrawal response is not observed. This is because a CD of the feeding command effectively inhibits the maladaptive withdrawal during feeding (Davis et al., 1973).

As another example, crayfish exhibit an escape response by flipping their tail when hair cells in their tail and abdomen are activated by an unexpected external stimulus. The same hair cell sensors are activated repeatedly during escape movements. However, CD from self-generated movement commands prevents reafference from activating the sensors, thereby preserving the salience of external stimuli (Krasne and Bryan, 1973).

Both of these examples are in invertebrates and belong to the category of "lower-order CD" where gating of sensory response is an all-or-none process. This type of mechanism causes a global suppression of sensory responsiveness by preventing both self-generated and externally induced stimuli from activating the

sensory receptors. Consequently, lower-order CD does not allow the distinction between self-generated and other-generated stimuli in the midst of an ongoing movement (Crapse and Sommer, 2008).

In contrast, “higher-order CD” allows an animal to detect an unexpected external event during an ongoing movement (Crapse and Sommer, 2008). For example, the mormyrid fish monitors the external aquatic environment by generating electric organ discharge (EOD) signals. Generation of EOD is accompanied by electric organ CD (EOCD) that reaches the electrosensory structure involved in the processing of reafference arising from electroreceptors. If there is no perturbation in the aquatic environment, the EOCD matches the reafferent feedback and blocks it. However, if there is discrepancy between EOCD and feedback due to the presence of an unexpected event in the environment, the fraction of the feedback that is unexpected is not gated and is allowed to reach downstream structures in the nervous system. Thereby, the mormyrid fish is able to identify unexpected events in the external environment while engaging in a motor behavior (Caputi, 2004).

Bats navigate in the environment by emitting high-intensity and high-frequency sound. CD associated with the self-generated sound is transmitted to the inferior colliculus where it is compared with the echo (i.e., acoustic feedback) to interpret the acoustic input. If there is a perturbation in the environment, the CD signal will not match the echo and the portion of the signal that does not match will be conveyed to higher-order centers to enable assessment of the size, location, and speed of the object that resulted in the discrepancy (Neuweiler, 2003).

Corollary discharge in development

Relatively little is known about the function of CD mechanisms in early infancy. In the context of infant rats, reafference from self-generated, high-amplitude wake movements is blocked in sensory structures including the external cuneate nucleus (ECN; Tiriac and Blumberg, 2016), thalamus (Tiriac et al., 2012), and somatosensory cortex (Mohns and Blumberg, 2010). Mechanistically, this suggests that wake movements are processed as if they are expected; therefore, CD associated with wake movements gates the reafference in those areas (Tiriac and Blumberg, 2016).

However, self-generated movements are not restricted to periods of wakefulness. Infants also exhibit spontaneous, jerky movements of skeletal muscles during periods of active sleep (AS; or REM sleep), which is the predominant behavioral state during early infancy (Roffwarg et al., 1966; Jouvet-Mounier et al., 1970). These spontaneous, self-generated movements, occurring exclusively during AS, are known as myoclonic twitches.

Twitching: a predominant motor behavior in developing animals

Myoclonic twitches are spontaneous, brief, jerky, and discrete movements of the limbs during AS (Seelke and Blumberg, 2008; Blumberg et al., 2013), and are among the most conspicuous behaviors during early infancy in a diversity of species (Roffwarg et al., 1966; Gramsbergen et al., 1970; Jouvet-Mounier et al., 1970; Blumberg et al., 2013). Twitches are expressed embryonically (Robinson et al., 2000; Milh et al., 2007; Robinson et al., 2008) and persist throughout the

lifespan (Gassel et al., 1964; Stefani et al., 2015). Twitches are abundant and observed throughout the body including the limbs and tail, as well as in facial muscles that control the movement of eyes, lips, and whiskers (Marcano-Reik et al., 2010; Petersson et al., 2003; Seelke and Blumberg, 2008; Tiriac et al., 2012; Blumberg et al., 2013). Unlike wake movements (i.e., kicking, stretching, etc.) that occur against a background of elevated muscle tone, twitches occur as discrete, singular events against a background of muscle atonia (Blumberg et al., 2013).

Importantly, reafference from twitches, unlike that from wake movements, triggers heightened activity in sensory structures including the spinal cord, brainstem, thalamus, and sensorimotor cortex (Khazipov et al., 2004; Mohns and Blumberg, 2010; Geborek et al., 2012; Tiriac et al., 2014; Inacio et al., 2016; Tiriac and Blumberg, 2016). For example, by recording from the ECN of week-old rats, evidence was found for sensory gating of reafferent feedback arising exclusively from self-generated wake movements. In contrast, reafference arising from self-generated twitches trigger robust activity in the ECN and downstream structures. This state-dependent gating of reafference from self-generated movements suggested that CD is suspended in the ECN during twitching. Accordingly, twitch-related reafference is processed *as if* it is unexpected (Tiriac and Blumberg, 2016).

Although apparently suspended in primary sensory areas, there is evidence that twitches are accompanied by CD. The evidence comes from recordings in the cerebellum (Sokoloff et al., 2015b; Sokoloff et al., 2015a), a structure that is strongly implicated in sensorimotor processing and integration in a diversity of species (Wolpert et al., 1998; Proville et al., 2014; Requarth and Sawtell, 2014).

Overview of cerebellar anatomy and firing properties

Purkinje cells (PCs) are the principal cells in the cerebellar cortex and its only output neurons. Afferent inputs to PCs arrive via one of two pathways originating from precerebellar nuclei: climbing fibers and mossy fibers (Fig 2; Eccles, 1967). Climbing fibers originate solely from the inferior olive (IO), located at the ventral brainstem (Desclin, 1974; Sugihara et al., 2001; Reeber et al., 2012). Spontaneous IO activity is conveyed to PCs in a one-to-one manner via climbing fibers (Ruigrok and Voogd, 2000) where it triggers complex spikes (Hausser and Clark, 1997). Complex spikes are characterized by a single large action potential followed by a rapid train of multiple spikes that occur at a frequency of ~1 Hz (Burroughs et al., 2017).

Mossy fibers, on the other hand, originate from several brainstem nuclei including the ECN, lateral reticular nucleus (LRN), and pontine nuclei (Ruigrok et al., 2014). Activity in these nuclei are conveyed to the PCs where they trigger simple spikes (Hausser and Clark, 1997). Unlike complex spikes, simple spikes are single action potentials occurring at a relatively higher frequency (~ 20-200 Hz; Burroughs et al., 2017).

In a recent study, spontaneous activity of cerebellar PCs was recorded in 8-day-old rats during sleep and wake (Sokoloff et al., 2015b). Consistent with previous work, it was found that the cerebellar PCs are more active during AS than wakefulness; however, when activity was triggered on twitches, a unique pattern was observed in their response. Both complex and simple spikes responded by

increasing their firing within 0-30 ms after a twitch, a latency shorter than that required for reafferent signals to reach the cerebellum from the periphery in rat pups (Puro and Woodward, 1977). These short latencies seemed consistent with the latencies expected for synaptic transmission of CD from motor areas to the cerebellum (Azim et al., 2014; Azim and Alstermark, 2015); accordingly, it was suggested that motor structures could be conveying twitch-related CD signals to the cerebellum, bypassing the periphery (Sokoloff et al., 2015b).

Corollary discharge in the precerebellar nuclei?

If CD reaches PCs via climbing and mossy fibers, one would expect to see evidence of CD in the precerebellar nuclei. As mentioned above, the IO is the sole source of the climbing fiber input (Ruigrok et al., 2014). In adults, the IO receives direct input from midbrain motor structures (De Zeeuw et al., 1998). IO activity often coincides with the onset of self-generated movements (Apps, 1999) and is suppressed in response to predicted sensory input (Gellman et al., 1985). Based on these observations, it has been proposed that the adult IO receives CD from self-generated movements (Devor, 2002). Accordingly, we hypothesized that the IO receives twitch-related CD in infant rats.

The mossy fiber inputs originate from several brainstem structures including the pontine nuclei, ECN, and the LRN (Ruigrok et al., 2014). First, the pontine nuclei are an unlikely source of CD in week-old rats because it receives motor input from the motor cortex (Lee and Mihailoff, 1990), which does not play a role in the production of twitches (Kreider and Blumberg, 2000; Blumberg, 2010). Second,

the ECN only receives sensory input from the periphery and exhibits neural responses to twitching that are consistent with that (Tiriac and Blumberg, 2016); therefore, the ECN can be ruled out as a potential source of CD to the cerebellum. Finally, the LRN receives both sensory input and motor input from midbrain structures (Alstermark and Ekerot, 2013; Pivetta et al., 2014). Moreover, it has been implicated in processing CD associated with self-generated movements in adults (Arshavsky et al., 1978; Alstermark and Ekerot, 2015). Therefore, we hypothesized that the LRN processes and conveys CD signals to the cerebellum via the mossy fibers.

In CHAPTER 2, we recorded spontaneous extracellular unit activity in the IO and LRN in unanesthetized, 7-9-day-old rats as they cycled normally between sleep and wake. In the majority of IO units and in a subset of LRN units, neural activity was particularly pronounced at the time of twitch onset. This twitch-related activity was remarkably sharp and precise, reaching a peak in firing rate within 0-10 ms after twitch onset. This unique pattern of peri-twitch activity suggested that, unlike sensory structures that receive reafference from twitches, these two precerebellar nuclei receive CD signals from areas involved in the production of twitches.

In CHAPTER 3, using anatomical tracing, immunohistochemistry, and extracellular electrophysiology, we identified non-overlapping premotor areas in the midbrain mesodiencephalic junction (MDJ) that are involved in the production of twitches and send CD to the IO and LRN; these areas include the rostral nucleus of Darkschewitsch, which projects to the IO, and the red nucleus, which projects to the LRN.

In CHAPTER 4, using a pharmacological manipulation, we show that calcium-activated-slow potassium (SK) channels are responsible for the sharp CD peak of IO activity in response to twitches.

Altogether, these results show for the first time that twitches are accompanied by CD that triggers activity in the IO and LRN. They also provide the first direct electrophysiological evidence of CD in a developing mammal. By providing converging sensory and motor input, twitches could facilitate somatotopic map formation and sensorimotor integration in the developing cerebellum. Moreover, by processing twitch-related CD and reafference, these findings suggest a mechanism whereby the developing nervous system learns to distinguish between self- and other-generated movements.

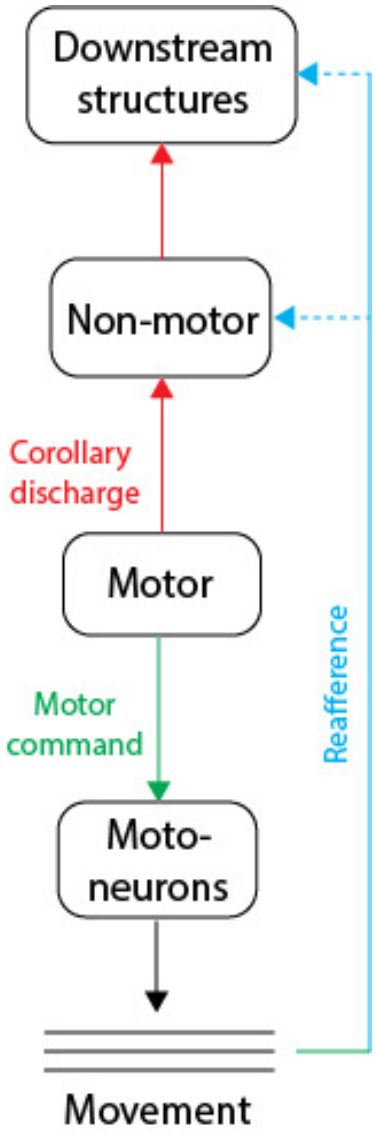

Fig 1. Schematic representation of pathways conveying movement-related information. Green, red, and blue arrows depict motor command, corollary discharge and reafference, respectively, associated with self-generated movements.

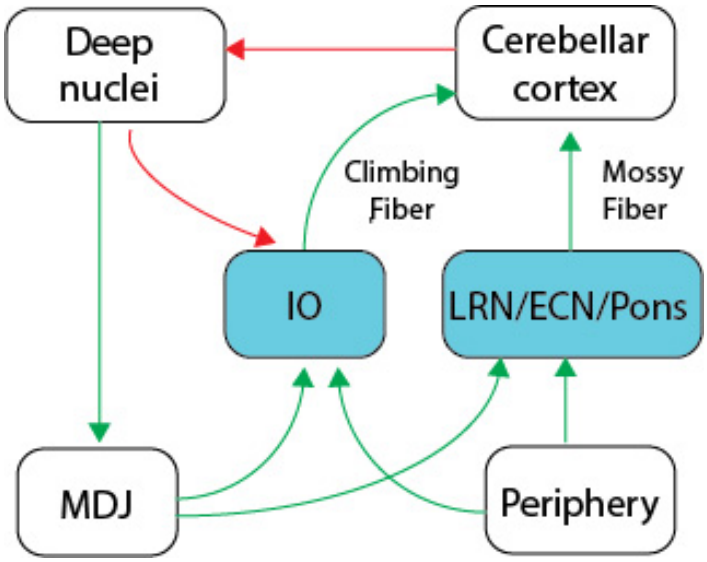

Fig 2. Schematic representation of basic cerebellar circuitry. Simplified diagram showing climbing fiber and mossy fiber inputs to the cerebellar cortex and its output through the deep nuclei. Green arrows indicate excitatory connections and red arrows indicate inhibitory connections. IO: inferior olive; LRN: lateral reticular nucleus; MDJ: mesodiencephalic junction.

CHAPTER 2

Spontaneous activity of the IO and LRN during sleep and wake in infant rats

As described in CHAPTER 1, we hypothesized that the IO and LRN receive twitch-related CD from motor areas. To test this hypothesis, we recorded spontaneous activity of the IO and LRN in unanesthetized and head-fixed infant rats as they cycled normally between sleep and wake (Fig 3A).

METHODS

All experiments were carried out in accordance with the National Institutes of Health Guide for the Care and Use of Laboratory animals (NIH Publication No. 80-23). Experiments were also approved by the Institutional Animal Care and Use Committee (IACUC) of the University of Iowa.

Subjects

Male and female Sprague-Dawley Norway rats *(Rattus norvegicus)* at postnatal day (P) 7-9 (hereafter P8; n=30) and at P11-12 (hereafter P12; n=6) from 36 litters were used for the study. All litters were culled to eight pups by P3. Mothers and litters were housed and raised in standard laboratory cages (48 x 20 x 26 cm). Food and water were available ad libitum. The animals were maintained on a 12-h light-dark cycle with lights on at 0700 h. Littermates were never assigned to the same experimental group.

Surgery

A pup with a visible milk band was removed from the home cage. Under isoflurane (3-5%) anesthesia, bipolar hook electrodes (50 µm diameter, California Fine Wire, Grover Beach, CA) were inserted into the nuchal, forelimb, and hindlimb muscles for electromyography (EMG) and secured with collodion. A stainless steel ground wire was secured transdermally on the back. A custom-built head-fix device was then secured to the exposed skull with cyanoacrylate adhesive (Blumberg et al., 2015). The local anesthetic, Bupivicaine (0.25%) was applied topically to the site of incision and some subjects were also injected subcutaneously with the analgesic agent carprofen (0.005 mg/g). The pup was lightly wrapped in gauze and allowed to recover in a humidified, temperature-controlled (35 ºC) incubator for at least one hour. After recovery, the pup was briefly (<15 min) re-anesthetized with isoflurane (2-3%) and secured in a stereotaxic apparatus. A hole was drilled in the skull for insertion of the recording electrode into the IO (coordinates: AP=3.4-3.6 mm caudal to lambda; ML=0-1.2 mm) or the LRN (coordinates: AP=3.5-3.7 mm caudal to lambda; ML=1.5-1.8 mm). Two additional holes were drilled over the frontal or parietal cortices for subsequent insertion of the ground wire and a thermocouple (Omega Engineering, Stamford, CT) to measure brain temperature. After surgery, the pup was transferred to the recording chamber.

Electrophysiological recordings

The head-fix device was secured to the stereotaxic apparatus housed within the recording chamber and the pup was positioned with its body prone on a narrow

platform with limbs dangling freely on both sides (Blumberg et al., 2015). Care was taken to regulate air temperature and humidity such that the pup's brain temperature was maintained at 36-37 ºC. Adequate time (1-2 h) was allowed for the pup to acclimate to the recording environment and testing began only when it started cycling normally between sleep and wake. Pups rarely exhibited abnormal behavior or any signs of discomfort or distress; when they did, the experiment was terminated. The bipolar EMG electrodes were connected to a differential amplifier (A-M Systems, Carlsborg, WA; amplification: 10,000x; filter setting: 300-5000 Hz). A ground wire (Ag/AgCl, 0.25 mm diameter, Medwire, Mt. Vernon, NY) was inserted into the frontal or parietal cortex contralateral to the recording site and a thermocouple was inserted into the frontal or parietal cortex ipsilateral to the recording site. Neurophysiological recordings were performed using a 16-channel silicon electrode or a 4-channel linear probe (A1x16-10mm-100-177; Q1x4-10mm-50-177, NeuroNexus, Ann Arbor, MI), connected to a data acquisition system (Tucker-Davis Technologies, Alachua, FL) that amplified (10,000x) and filtered (500-5000 Hz) the neural signals. A digital interface and Spike2 software (Cambridge Electronic Design, Cambridge, UK) were used to acquire EMG and neurophysiological signals at 1 kHz and at least 12.5 kHz, respectively.

A micromanipulator (FHC, Bowdoinham, ME) was used to lower the electrode into the brain (DV; IO: 5.5-6.2 mm, LRN: 5-5.8 mm) until action potentials were detected. Recording began at least 10 min after multiunit activity (MUA) was detected. Before insertion, the electrode was dipped in fluorescent DiI (Life Technologies, Grand Island, NY) for later identification of the recording sites.

Recording of MUA and EMG activity continued for 30 min as the pup cycled freely between sleep and wake (in two pups, activity was recorded for only 15 min). The experimenter, blind to the electrophysiological record, scored the pup's sleep and wake behaviors, as described previously (Karlsson et al., 2005).

At the end of the recording session, the experimenter assessed evoked neural responses to exafferent stimulation of the limbs. Forelimbs and hindlimbs were gently stimulated using a paint brush. When evoked responses were observed in at least one of the recording channels, stimulation was repeated 20-30 times at intervals of at least 5 s. Each stimulus event was marked using a key press.

Histology

At the end of all recording sessions, pups were anesthetized with sodium pentobarbital (1.5 mg/g IP) or ketamine/xylazine (0.02 mg/g IP) and perfused transcardially with phosphate-buffered saline and 4% formaldehyde. Brains were sectioned coronally at 80 µm using a freezing microtome (Leica Microsystems, Buffalo Grove, IL). Recording sites were determined by examining DiI tracks, before and after staining with cresyl violet, using a fluorescent microscope (Leica Microsystems, Buffalo Grove, IL).

Data analysis

Spike sorting. As described previously (Sokoloff et al., 2015b; Mukherjee et al., 2017), action potentials (signal-to-noise ≥ 2:1) were sorted from MUA records using template matching and principal component analysis in Spike2 (Cambridge

Electronic Design). Waveforms exceeding 3.5 SD from the mean of a given template were excluded from analysis.

Identification of behavioral states. EMG activity and behavioral scoring were used to identify behavioral state (Blumberg et al., 2015). To establish an EMG threshold for distinguishing sleep from wake, EMG signals were rectified and smoothed (tau = 0.001 s). The mean amplitude of high muscle tone and atonia were calculated from five representative 1-s segments and the midpoint between the two was used to establish the threshold for defining periods of wake (defined as muscle tone being above the threshold for at least 1 s) and sleep (defined as muscle tone being below the threshold for at least 1 s). Active wake (AW) was identified by high-amplitude limb movements (e.g., stepping, stretching) against a background of high muscle tone and was confirmed using behavioral scoring. Active sleep (AS) was characterized by the presence of myoclonic twitches of the limbs against a background of muscle atonia. Twitches were identified as sharp EMG events that exceeded by ≥ 3x the mean EMG baseline during atonia; twitches were also confirmed by behavioral scoring (Seelke and Blumberg, 2010). Additionally, behavioral quiescence (BQ) was characterized as periods of low muscle tone interposed between AW and AS.

State-dependent neural activity. For each unit, average firing rate across all behavioral states was determined. Bouts of AS, AW, and BQ were excluded when firing rates exceeded 3 SD of the firing rate for that behavioral state; this happened rarely (0-2 per unit). Next, pairwise comparison of firing rates across states was performed using the Wilcoxon matched-pairs signed-ranks test (SPSS; IBM,

Armonk, NY). Units were categorized as AS-on (AS > AW ≥ BQ), AW-on (AW > AS ≥ BQ), AS+AW-on (AS = AW > BQ) or state-independent (AS = AW = BQ). Firing rates of all AS-on units across behavioral states were further compared using the Wilcoxon matched-pairs signed-ranks test.

Twitch-triggered neural activity. To determine the relationship between unit activity and twitching, we triggered unit activity on twitch onsets and generated perievent histograms over a 1-s window using 5- or 10-ms bins. We performed these analyses on each individual unit using twitches from nuchal, forelimb, and hindlimb muscles. We tested statistical significance by jittering twitch events 1000 times over a 500-ms window using Patternjitter (Harrison and Geman, 2009; Amarasingham et al., 2012). Then using a custom-written Matlab (Mathworks) program, we generated upper and lower confidence bands ($p<0.05$ or 0.01 for each confidence band) using a method that corrects for multiple comparisons (Amarasingham et al., 2012). For each unit, after histograms were separately constructed for nuchal, forelimb, or hindlimb twitches, we identified activity that was significant in response to a twitch. When more than one muscle yielded a significant change in neural activity, we further analyzed the data only for the muscle that showed the strongest relationship (determined by the highest firing rate) between twitches and unit activity. We then pooled these data to create perievent histograms composed of significant units and performed jitter analyses on the pooled data.

Evoked response to exafferent stimulation. We identified MUA in which evoked responses were observed and then sorted the units. Those units were then pooled

and triggered on stimulus onset (determined using EMG artifact) to create perievent histograms. The jitter analysis was performed on the pooled data, as described above.

Unless otherwise stated, alpha was set at 0.05.

RESULTS

Olivary activity predominates during active sleep

Results from P8 pups are described first. Electrode placement within the IO was confirmed histologically (Figure 3B). Recording sites were located within the dorsal accessory olive (DAO; n=19 units across 12 pups) or the medial accessory olive (MAO) and the principal olive (PO; n=18 units across 8 pups; Figure 3C). Overall, the unit activity was phasic and was largely restricted to periods of AS; also, activity appeared to be suppressed immediately after the onset of AW. Sparse activity was observed during BQ (Fig 3D). The majority (69%, n=24) of IO units were AS-on (Fig 3E), and the mean firing rate of the AS-on units (2.9 ± 0.4 Hz) was approximately three times higher than that for the other two states ($p<0.005$; Fig 3F).

Twitches trigger precise, zero-latency olivary activity

The phasic IO activity clustered around periods of myoclonic twitching. Therefore, we examined the temporal relationship between twitches and unit activity by

creating perievent histograms (1-s windows, 5-ms bins) with unit activity triggered on twitch onset.

First, in a motor structure like the RN (green trace in Figure 4A), unit activity increases 20-40 ms before the onset of a twitch (Del Rio-Bermudez et al., 2015). Second, in a sensory structure like the ECN (blue trace in Figure 4A), unit activity increases at least 10-50 ms after the onset of a twitch (Tiriac and Blumberg, 2016).

In the IO, however, we found neither of these patterns. Instead, the majority of IO units (62%, n=23) were active within $\pm$10 ms of the onset of a twitch (Fig 4B, C). These activity profiles were very sharp; indeed, they were strikingly different from those observed in any of the motor and sensory structures from which we have previously recorded (e.g., see Fig 4D). Finally, the IO units that exhibited this profile were responsive primarily to nuchal and/or forelimb twitches, and rarely to hindlimb twitches (Fig 5A-D).

There are three possible explanations for these sharply peaked activation patterns observed in IO units: (a) the IO is part of the motor pathway, (b) the IO receives reafference from twitches, or (c) the IO receives CD from a motor structure that produces twitches.

With respect to (a), the IO, despite being implicated in the precise timing of motor behaviors (De Zeeuw et al., 1998), is not directly involved in the generation of movements (Gellman et al., 1985). Although it receives afferent projections from motor areas (Saint-Cyr and Courville, 1981; Saint-Cyr, 1983), there are no efferent projections from the IO to spinal motor neurons. In fact, the sole efferent projection

from the IO comprises the climbing fibers that innervate cerebellar Purkinje cells (Ruigrok et al., 2014). Consequently, stimulation of the IO does not evoke or modulate movements (Gellman et al., 1985).

With respect to (b), although it is possible that the IO can receive short-latency reafferent signals (Sedgwick and Williams, 1967; Gellman et al., 1983), it is unlikely that reafference can account for the short-latency peaks observed here. First, when we have previously seen clear evidence of reafferent processing of sensory input (e.g., in the ECN, sensorimotor cortex), we have also seen clear evidence of exafferent responses (Tiriac et al., 2014; Tiriac and Blumberg, 2016). However, of the 23 IO units that exhibited sharp peaks with a latency of $\pm$10 ms, none responded to exafferent stimulation. In contrast, of the 7 IO units that exhibited twitch-triggered responses at latencies consistent with reafferent processing (i.e., ≥ 15 ms; Fig 6), 3 also responded to exafferent stimulation.

Accordingly, the signature feature of IO activity—in particular, the zero-latency peak and the sharp rise and fall in activity—are consistent with the notion that the IO receives CD associated with the production of a twitch.

Additionally, we recorded from the IO in a subset of P12 pups (Fig 7A). The overall firing rate was significantly higher at P12 than P8 (Fig 7B). As depicted in Fig 7C-E, we identified units showing zero-latency sharp peak around twitches at P12, however, the percentage (20%, n=2/10) was lower than that at P8. Instead, the percentage of units exhibiting broader peak with longer latency (60%, n=6/10)

increased suggesting a developmental emergence of sensory response in the IO at this age.

Having identified a phenotype of twitch-related CD signaling in the IO, we now know what to expect in other structures, like the LRN, that may similarly process CD. Moreover, because the LRN also receives sensory inputs from the periphery (Fig 8A; Alstermark and Ekerot, 2013), we would also expect to see evidence of reafference in that structure.

Corollary discharge and reafference from twitches trigger LRN activity

We confirmed electrode placements in the LRN (n=10 pups, 27 units, 1-6 units/pup; Fig 8B). Similar to the IO, the unit activity in the LRN was phasic, restricted to periods of AS and especially observed around the occurrence of twitches. LRN activity was sparse during BQ and was suppressed after AW-onset (Fig 8C). The majority (59%, n=16) of LRN units were AS-on (Fig 8D), and the mean firing rate of the AS-on units (1.4 ± 0.2 Hz) was approximately three times higher than that for the other two states ($p<0.001$; Fig 8E).

Next, we assessed the temporal relationship between unit activity and twitches by creating perievent histograms (1-s windows, 5-ms bins). Regardless of state-dependency, the majority of LRN units (88%, n=24) showed significant increases in firing rate in response to a twitch (Fig 8F). As predicted, we observed two different patterns of twitch-triggered activity. First, we found a subpopulation of LRN units (44%, n=12) that, like the majority of IO units, exhibited a sharp peak

within ±10 ms of a twitch (Fig 8G, left); also, these LRN units did not respond to exafferent stimulation of the limbs (data not shown).

Second, the remaining LRN units (44%, n=12) exhibited broader twitch-related activity profiles consisting of a peak in activity around twitch onset (±10 ms) and/or a peak with a latency of at least 15 ms (Figure 8G, right). The latter peak is what is expected from a short-latency reafferent responses (Tiriac et al., 2014; Tiriac and Blumberg, 2016). Indeed, 6 of these 12 units also responded to exafferent stimulation of either the forelimb or hindlimb with an average latency of 40 ms (Figure 8H).

Altogether, results from these experiments provide evidence that twitches are accompanied by CD signals that trigger activity in the majority of IO units and in a subpopulation of LRN units. By performing a subsequent experiments, we identify the potential sources of CD signal in these two precerebellar nuclei.

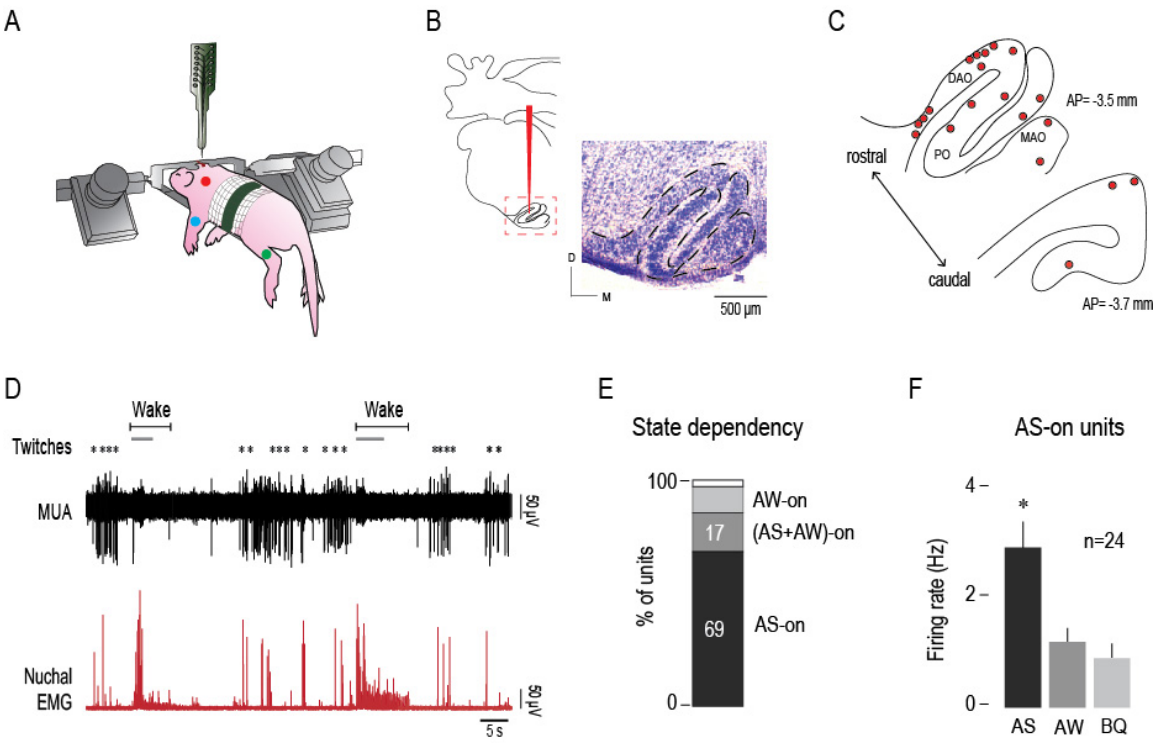

Fig 3. Olivary activity predominates during active sleep. (**A**) Illustration of a head-fixed rat pup in a recording apparatus instrumented with nuchal (blue), forelimb (red), and hindlimb (green) EMG electrodes. (**B**) Left: Reconstruction of a representative electrode placement within the IO (red vertical line). Red dashed line circumscribes the IO. Right: Coronal section (5x) stained with cresyl violet depicting the anatomical location of the IO (black dashed line). (**C**) Reconstruction of electrode placements (red circles) within the IO in two coronal sections across all subjects. (**D**) Representative recording of rectified nuchal EMG activity and multiunit activity (MUA) in the IO during spontaneous sleep-wake cycling. Asterisks denote twitches and gray horizontal bars denote wake movements as scored by the experimenter. (**E**) Stacked plot depicting the percentage of units that were AS-on, (AS+AW)-on, and AW-on units in the IO. (**F**) Bar graphs showing mean (+SEM) firing rates of AS-on units across behavioral states. * significant difference from

AW and BQ, $p<0.005$. D=dorsal; M=medial; DAO=dorsal accessory olive; MAO=medial accessory olive; PO=principal olive; AP=antero-posterior in relation to lambda; AS=active sleep; AW=active wake; BQ=behavioral quiescence.

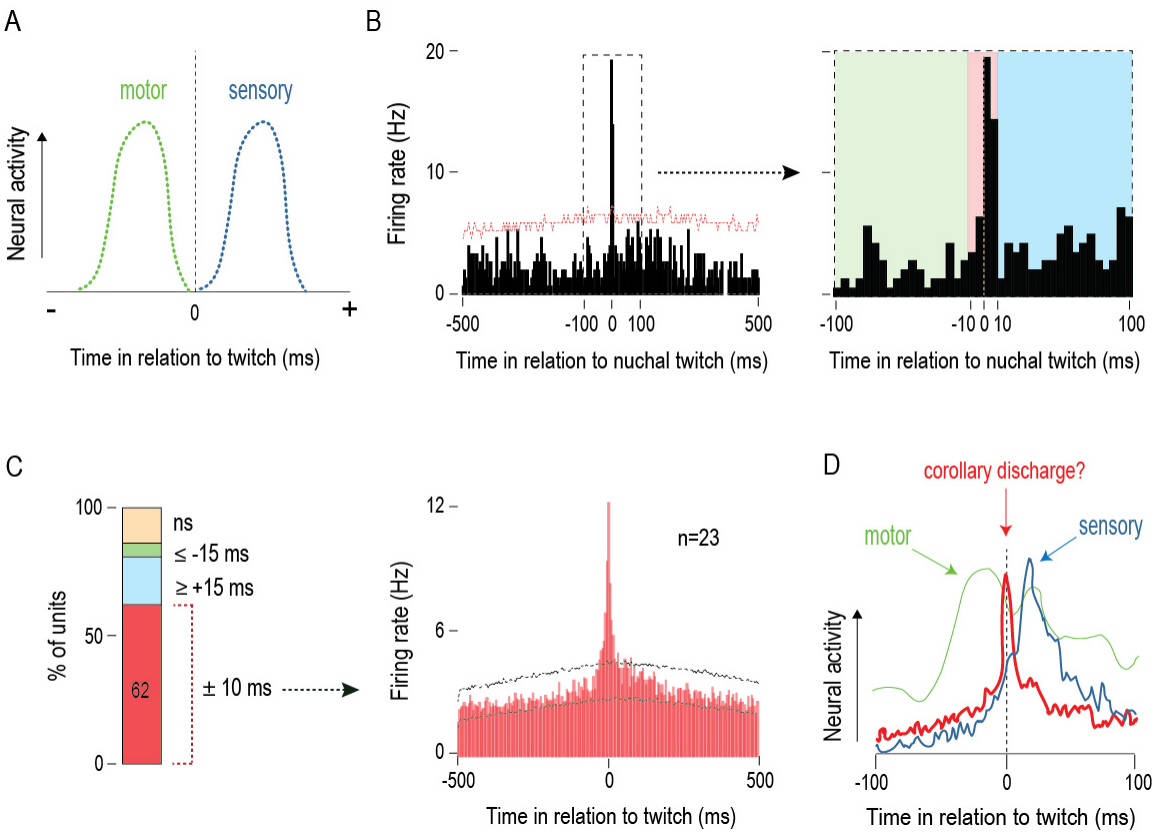

Fig. 4. Twitches trigger sharp, zero-latency olivary activity. (**A**) Perievent histograms for idealized motor and sensory units in relation to twitch onset. Motor activity precedes the onset of twitches (green line) and reafference follows the onset of twitches (blue line). Black vertical line denotes twitch onset. (**B**) Left: Perievent histogram (5-ms bins) showing sharp, zero-latency firing of a representative IO unit in relation to nuchal muscle twitches. Upper confidence band ($p<0.01$ for each band) is indicated by red horizontal dashed line (lower confidence band is at zero). Black dashed box demarcates the ±100-ms time window around twitches. Right: The ±100-ms time window around twitches at left is shown. Green, red, and blue shaded areas denote ≤-15-ms, ±10-ms, and ≥15-ms time windows, respectively. (**C**) Left: Stacked plot showing the percentage of IO units that

exhibited significant increases in firing within ±10-ms (red), ≥15-ms (blue), and ≤-15-ms (green) time windows around twitches. Right: Perievent histogram showing cumulative IO unit activity in relation to twitches for those units that were significantly active in the ±10-ms time window. Data are pooled across 23 units. Upper and lower confidence bands ($p<0.01$ for each band) are indicated by red and gray horizontal dashed lines, respectively. (**D**) Comparison of IO activity in relation to twitches (red; from C) with that of a representative motor (green line; adapted from Del Rio-Bermudez et al., 2015) and sensory (blue line; adapted from Tiriac and Blumberg, 2016) structure. Black vertical dashed line denotes twitch-onset.

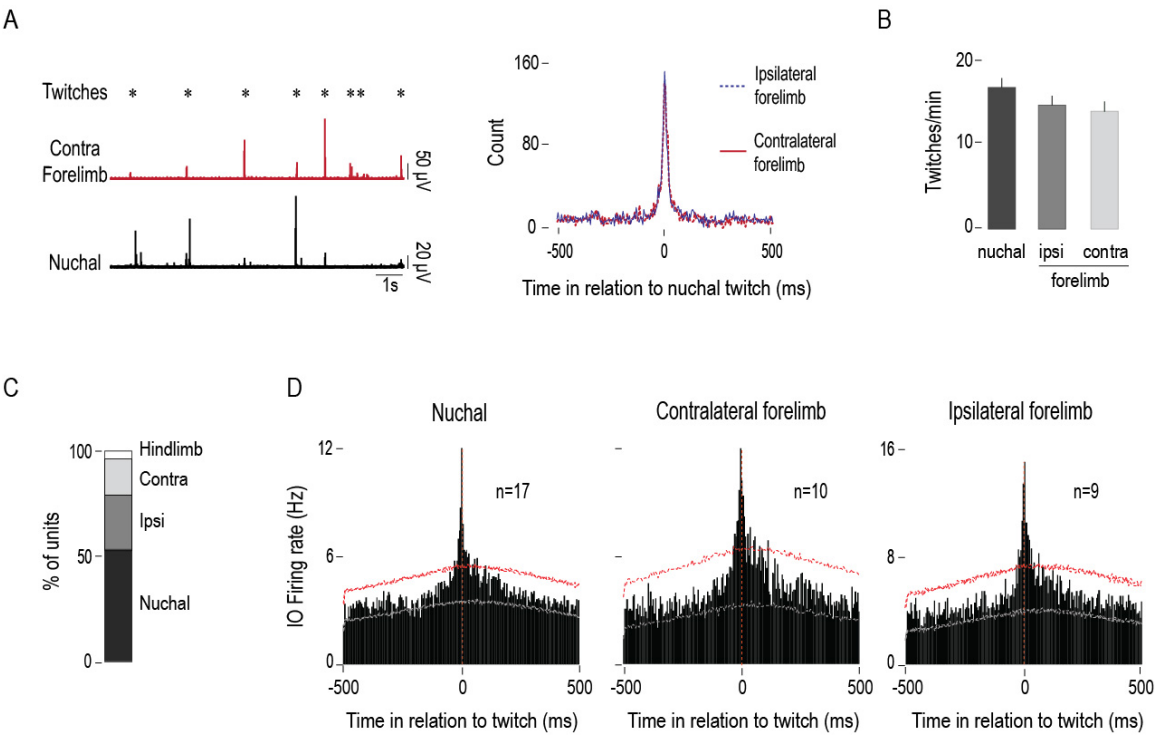

Fig. 5. IO units respond predominantly to nuchal and forelimb twitches. (**A**) Left: Representative recording of nuchal and contralateral forelimb EMG activity showing co-occurrence of twitches in those muscles. Asterisks denote experimenter-scored twitches. Right: Cross-correlogram (5-ms window) depicting co-occurrence of nuchal muscle twitches with contralateral (red line) and ipsilateral (blue dotted line) forelimb twitches. (**B**) Bar graphs depicting mean (+SEM) rates of twitching in nuchal muscle and ipsilateral and contralateral forelimb muscles. Data are pooled across 15 pups (**C**) Stacked plot showing the percentage of IO units that exhibited sharp, zero-latency activity in relation to nuchal, ipsilateral forelimb, contralateral forelimb, and hindlimb twitches. (**D**) Perievent histograms showing cumulative IO unit activity in relation to nuchal muscle and contralateral and ipsilateral forelimb twitches. Data are pooled across 17, 10, and 9 units, respectively. Upper and lower confidence bands ($p<0.01$ for each band) are

indicated by red and gray horizontal dashed lines, respectively. ipsi: ipsilateral; contra: contralateral.

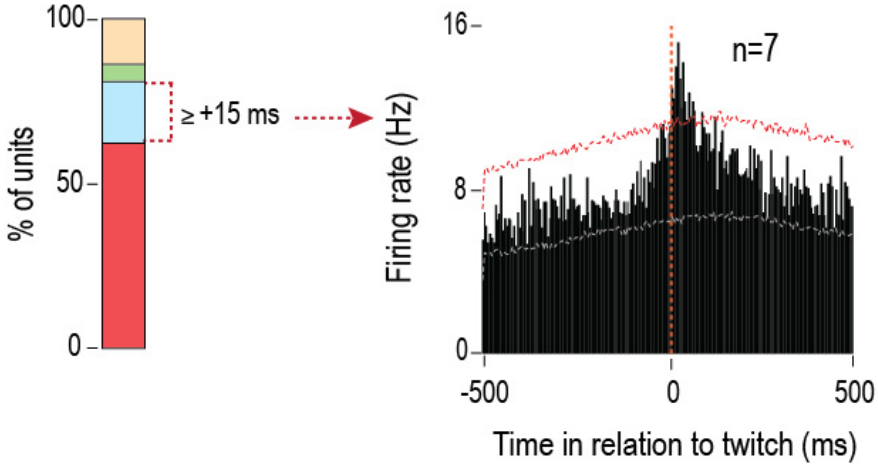

Fig. 6. Sensory responses of IO units. Left: Stacked plot showing the percentage of IO units that exhibited significant increases in firing rates within defined time windows around twitches. Right: Perievent histogram showing cumulative IO unit activity in relation to twitches for the ≥15-ms time window (blue stack at left). Data are pooled across 7 units. Upper and lower confidence bands ($p<0.01$ for each band) are indicated by red and gray horizontal dashed lines, respectively. ns: not significant.

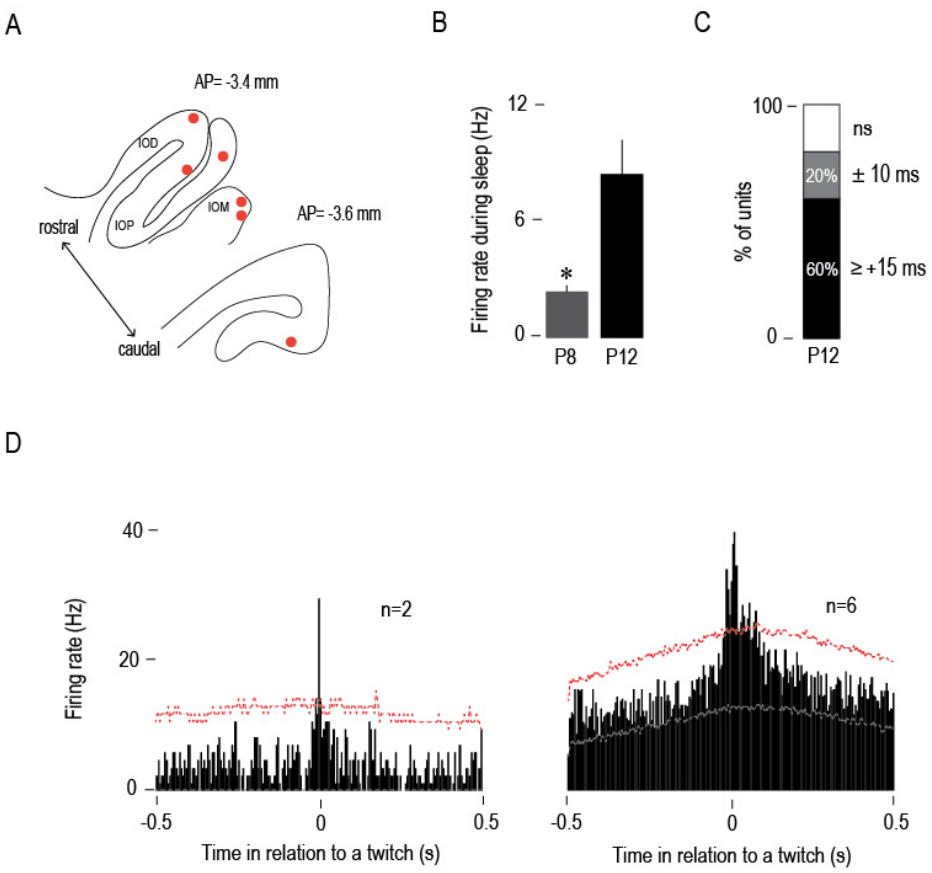

Fig 7. Spontaneous IO activity at P12. (**A**). Reconstruction of electrode placements (red circles) within the IO in two coronal sections for all subjects. (**B**) Bar graphs showing mean (+SEM) unit firing rates during sleep at P8 and P12. * significant difference from P12, $p<0.001$ (**C**) Stacked plot showing the percentage of IO units that exhibited significant increases in firing rate in the ≥15-ms (black) and ±10-ms (gray) time windows around twitches at P12. (**D**) Perievent histograms showing cumulative IO unit activity in relation to twitches; Left: data pooled across the 2 units that significantly increased their activity in the ±10-ms time window (gray stack in C). Right: data pooled across the 6 units that significantly increased their activity in the ≥15-ms time window (black stack in C). Upper and lower confidence

bands ($p<0.01$ for each band) are indicated by red and gray horizontal dashed lines, respectively.

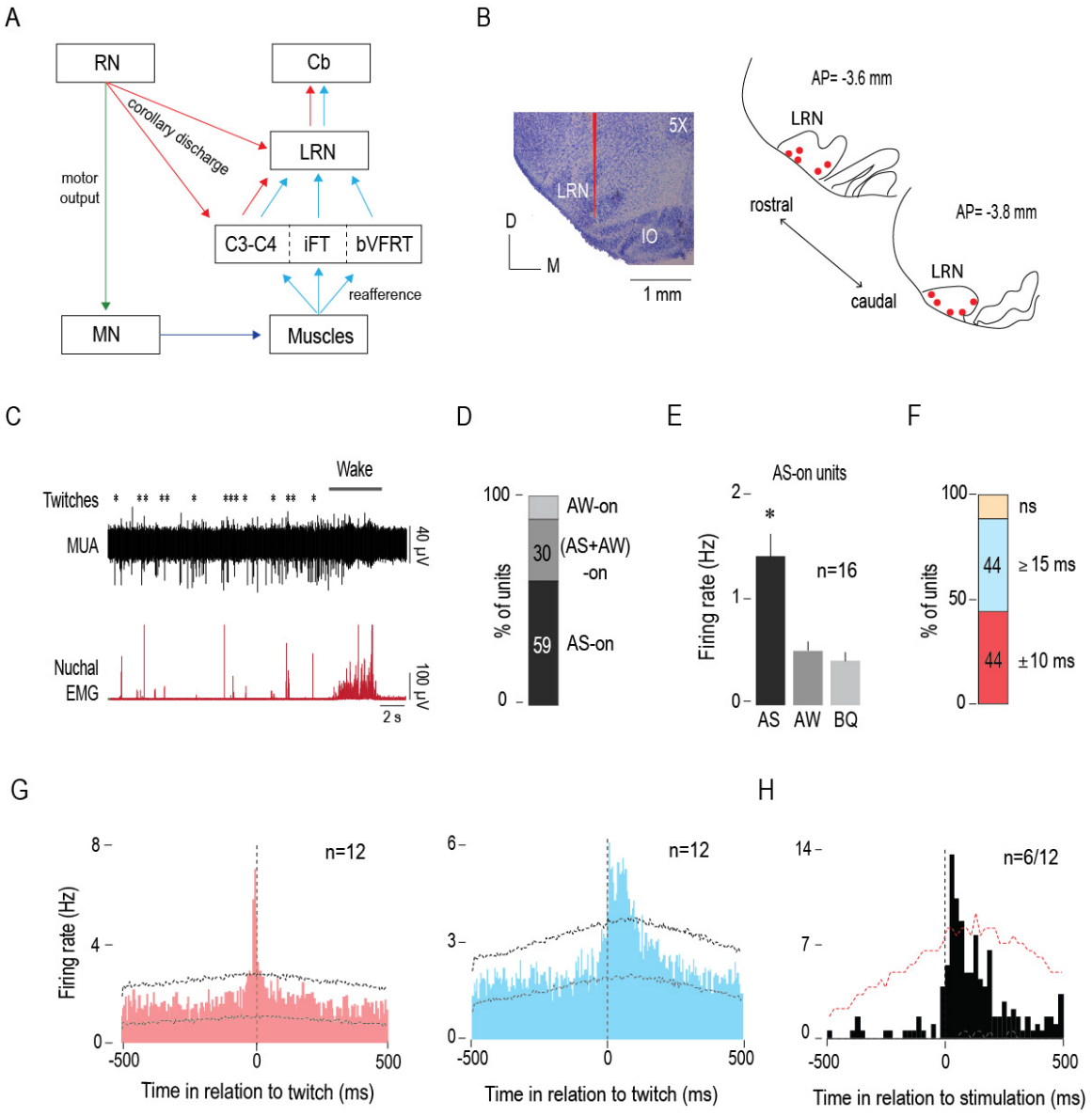

Fig 8. The LRN receives twitch-related corollary discharge and reafference signals. (**A**) Diagram depicting afferent and efferent connections of the LRN. Pathways conveying motor commands (green), reafference (blue), and corollary discharge (red) are shown (adapted from Alstermark and Ekerot, 2013). (**B**) Left: Coronal section (5x) stained with cresyl violet depicting the anatomical location of

the LRN in the brainstem and reconstruction of a representative electrode placement (red vertical line) in the LRN. Right: Reconstruction of electrode placements (red circles) within the LRN in two coronal sections across all P8 subjects (n=10). (**C**) Representative recording of rectified nuchal EMG activity and multiunit activity (MUA) in the LRN during spontaneous sleep-wake cycling. Asterisks denote twitches and gray horizontal bars denote wake movements as scored by the experimenter. (**D**) Stacked plot showing the percentage of AS-on, (AS+AW)-on, and AW-on units in the LRN. (**E**) Bar graphs showing mean (+SEM) firing rates of AS-on units across behavioral states. * significant difference from AW and BQ, $p<0.001$. (**F**) Stacked plot depicting the percentage of units that significantly increased their firing rates ±10 ms around twitches (red) and ≥15 ms following twitches (blue). (**G**) Perievent histograms (5-ms bins) showing cumulative LRN unit activity in relation to twitches. Left: Data pooled across 12 units that significantly increased their activity in the ±10-ms time window (red). Right: Data pooled across 12 units that significantly increased their activity in the ≥15 ms time window (blue). Black vertical dashed lines indicate twitch onset. Upper and lower confidence bands ($p<0.01$ for each band) are indicated by black and green horizontal dashed lines, respectively. (**H**) Perievent histogram (20-ms bins) depicting cumulative LRN unit activity (n=6 of a possible total of 12) in response to forelimb or hindlimb stimulation for those units that significantly increased their activity in the ≥15 ms time window (blue histogram in G). Black vertical dashed line corresponds to stimulation onset determined using EMG activity. Upper confidence band ($p<0.05$) is indicated by red horizontal dashed line. RN: red

nucleus; MN: motor neurons; C: cervical segment; LRN: lateral reticular nucleus; Cb: cerebellum; IO: inferior olive; D: dorsal; M: medial; AP: antero-posterior in relation to lambda; AS: active sleep; AW: active wake; BQ: behavioral quiescence; ns: not significant.

CHAPTER 3

Midbrain premotor structures send twitch-related corollary discharge to the IO and LRN

We demonstrated in CHAPTER 2 that twitches are accompanied by CD signals that are conveyed to the IO and LRN. These signals should arise from premotor structures that are involved in the production of twitches. Both IO and LRN receive projections from premotor structures in the mesodiencephalic junction (MDJ) in adults (Alstermark and Ekerot, 2013; De Zeeuw et al.,1998). Moreover, the RN, one of the structures in the MDJ has been shown to be involved in twitch-production in P8 rats (Del Rio-Bermudez et al., 2015). Accordingly, we hypothesized that one or more structures in the MDJ convey twitch-related CD to the IO and LRN. To test this hypothesis, we performed anatomical tracing, immunohistochemistry and extracellular recordings in P8 rats.

Retrograde tracing

Retrograde tracing was performed at P8 (n=7 pups from 7 litters) using wheat germ agglutinin (WGA) conjugated to Alexa Fluor 555 or 488 (Invitrogen Life Technologies, Carlsbad, CA). WGA-555 was injected into the IO in 3 pups and into the LRN in 2 pups. In the remaining 2 pups, dual tracing was performed by injecting WGA-488 into the IO and WGA-555 into the LRN. To perform these injections, a pup was anesthetized with 2-5% isoflurane and secured in a

stereotaxic apparatus. A 0.5 µl microsyringe (Hamilton, Reno, NV) was lowered stereotaxically into the IO or LRN and 0.01-0.02 µl of 2% WGA-555 or WGA-488 (dissolved in 0.9% saline) was injected over 1 min. After a 15-min post-infusion period, the microsyringe was withdrawn and the incision was closed using Vetbond (3M, Maplewood, MN). The pup was returned to its home cage and perfused 24 h later as described above. Brains were sectioned coronally at 50 µm. Every other section was kept for Nissl staining for verification of the injection sites and areas that show retrograde labeling. Retrogradely labeled cell bodies were imaged using a fluorescent microscope (Leica Microsystems, Buffalo Grove, IL).

RESULTS

Independent structures in the mesodiencephalic junction project to the IO and LRN

The extent of diffusion of WGA around the injection sites in individual pups is reconstructed in coronal sections (Fig 9). Retrograde tracing from the IO (n=5; Fig 10A) revealed robust labeling of cell bodies in the MDJ, including the rostral interstitial nucleus of Cajal (RI), nucleus of Darkschewitsch (Dk), accessory oculomotor nuclei (MA3), and other diffuse areas in the MDJ. Little or no labelling was observed in the RN. In contrast, retrograde tracing from the LRN (n=4; Fig 10B) revealed robust labeling in the contralateral RN but not in other MDJ nuclei. Finally, when the two tracers were injected separately into the IO and LRN of the

same pup (n=2; Fig 10C), we found that the LRN-projecting cell bodies were located within the RN and the IO-projecting cell bodies were located outside the RN. These findings are consistent with those in adult rats (Ruigrok et al., 2014) and suggest that the major afferent connections to the IO and LRN arise from non-overlapping structures in the MDJ at this age.

Interestingly, MDJ nuclei that project to the IO and LRN also innervate spinal motor neurons. For example, the same MDJ nuclei that innervate the IO (Saint-Cyr and Courville, 1981; De Zeeuw et al., 1998) also project to the spinal cord (Zuk et al., 1983; Lakke, 1997) and are involved in hand, head, and eye movements (Fukushima, 1991; Onodera and Hicks, 1996). Similarly, the magnocellular part of the RN projects to spinal motor neurons (Onodera and Hicks, 2009) and is involved in the generation of movements (Williams et al., 2014; Morris et al., 2015), including twitches (Del Rio-Bermudez et al., 2015). Therefore, these MDJ structures have the capacity to send both motor commands to the spinal cord and CD signals to the IO and LRN.

To assess functional connectivity between MDJ neurons and the IO or LRN, we electrically stimulated the RN (n=4) and other MDJ nuclei (n=4) while monitoring forelimb and hindlimb movements in urethanized P8 rats. Subsequently, we performed immunohistochemistry to determine the expression of the c-Fos protein, a marker of neural activity (Chung, 2015), in the IO, LRN, and other structures.

Stimulation of midbrain structures

In urethanized (1.5 mg/g) head-fixed P8 rats (n=8 pups from 8 litters), a parylene-coated tungsten stimulating electrode (World Precision Instruments, Inc., Sarasota, FL) was lowered into the MDJ nuclei most strongly implicated by retrograde tracing. The nuclei were electrically stimulated to produce discrete movements of the forelimbs and/or hindlimbs (Fig 11A). Trains of pulses (pulse duration: 0.2-0.4 ms; pulse frequency: 300 Hz; train width: 45 ms; Williams et al., 2014) were delivered every 5 s for 60 min. The current was adjusted (300-900 μA) as needed to ensure that stimulation continued to reliably produce movement. Ninety min after the last stimulation, the pup was sacrificed and the brain was prepared for c-Fos immunohistochemistry.

Immunohistochemistry for c-Fos expression

Brains were sliced in 50 μm sections and every other section was kept for Nissl staining for verification of the stimulation sites and visualization of c-Fos expression, respectively. Primary antibody against c-Fos (anti-c-Fos rabbit polyclonal IgG; Santa Cruz Biotechnology) was diluted 1:1000 in a universal blocking serum (2% BSA/1% triton/0.02% NaAz) and applied to the sections. Sections were coverslipped and left to incubate for 48 h at 4˚C. After incubation of the primary antibody and a series of washes in PBS, a secondary antibody (Alexa Fluor 488 donkey anti-rabbit IgG; Life Technologies, Grand Island, NY; 1:500 in PBS) was applied to the section and incubated for 90 min at room temperature.

The slides were coverslipped using Fluorogel and expression of c-Fos was examined using a fluorescent microscope (Leica Microsystems, Buffalo Grove, IL).

RESULTS

MDJ stimulation produces limb movements and causes c-Fos activation in the IO and LRN

Stimulation of several non-RN MDJ nuclei produced ipsilateral and contralateral forelimb and hindlimb movements (Fig 11A) and resulted in c-Fos expression in the ipsilateral IO but not the LRN (Fig 11B). Similarly, stimulation of the RN produced contralateral forelimb movements (Fig 11A) and resulted in c-Fos expression in the contralateral LRN but not the IO (Fig 11C). These results indicate that MDJ nuclei are functionally connected to the IO and LRN at these ages.

It is possible that the c-Fos activation in the IO and LRN was due to sensory feedback arising from the stimulated movements. However, we observed little or no c-Fos expression in sensory areas like the cuneate nucleus and external cuneate nucleus (data not shown). These results suggest that c-Fos expression in the IO and LRN resulted directly from MDJ outputs to those structures.

It has been established that the RN is involved in the production of twitches (Del Rio-Bermudez et al., 2015) and, as shown here, in the conveyance of CD to the LRN. Similarly, if MDJ neurons outside of the RN convey twitch-related CD to the IO, we would also expect these neurons to be involved in the production of

twitches (Fig 12A). Therefore, we characterized the spontaneous activity of non-RN MDJ structures in P8 rats during sleep and wake. We aimed to record from MDJ neurons located in regions implicated earlier as projecting to the IO and, upon stimulation, producing limb movements (see Fig 10 and 11).

Electrophysiology

Using the methods described in CHAPTER 1, we recorded from the MDJ structures (coordinates; AP=4.7-4.9 mm caudal to bregma; ML=0.2-0.5 mm; DV=4.5-4.9 mm) outside and adjacent to the RN, in 7 pups from 7 litters using silicone recording electrodes.

RESULTS

MDJ neurons adjacent to the RN are active before and after the production of twitches

Electrode placements in the MDJ immediately medial to the RN were confirmed (n=7 pups, 1-5 units/pup; Fig 12B). The spontaneous activity of neurons in this region appeared mostly around twitches and wake movements (Fig 12C). When twitch-triggered perievent histograms (1-s window, 10-ms bins) were created, we found that the majority of the recorded units (88%, n=15 units) showed significant twitch-dependent activity (Fig 12D).

The temporal relationship between this neural activity and twitches revealed two primary subpopulations of units (Fig 12D). First, there were units that significantly increased their firing rates before the onset of a twitch (hereafter called twitch-preceding units) and second, there were units that significantly increased their firing rates after the onset of a twitch (hereafter called twitch-following units). The twitch-preceding units (59%, n=10 units across 5 pups) showed an increase in firing rate 10-70 ms before a twitch (Fig 12E, left). Interestingly, the majority of these twitch-preceding units (70%, n=7) also exhibited an increase in firing rate 10-50 ms after a twitch, suggesting they also receive reafference from a twitch. The twitch-following units (29%, n=5 units across 3 pups) showed an increase in firing rate 20-40 ms after a twitch (Fig 12E, right), suggesting they only receive reafference from a twitch. In terms of pattern and latency of twitch-triggered activity, these neurons behave similarly to those described previously in the RN (Fig 12F; Del Rio-Bermudez et al., 2015).

All together, results from this chapter provide converging evidence that independent premotor structures in the MDJ are involved in the production of twitches and send CD signals to the IO and LRN.

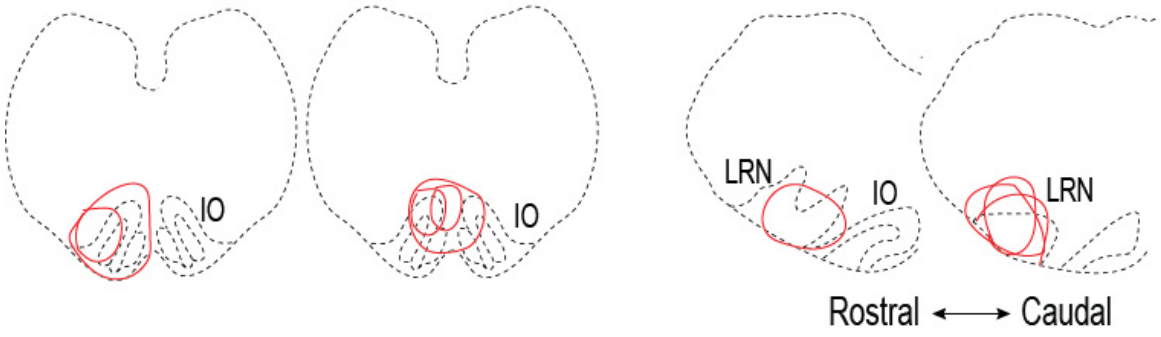

Fig 9. Diffusion of WGA injected into the IO and LRN. Reconstruction of coronal sections showing diffusion of WGA (488 or 555; red circles) injected into the IO and LRN of individual P8 rats. IO: inferior olive; LRN: lateral reticular nucleus; WGA=wheat germ agglutinin.

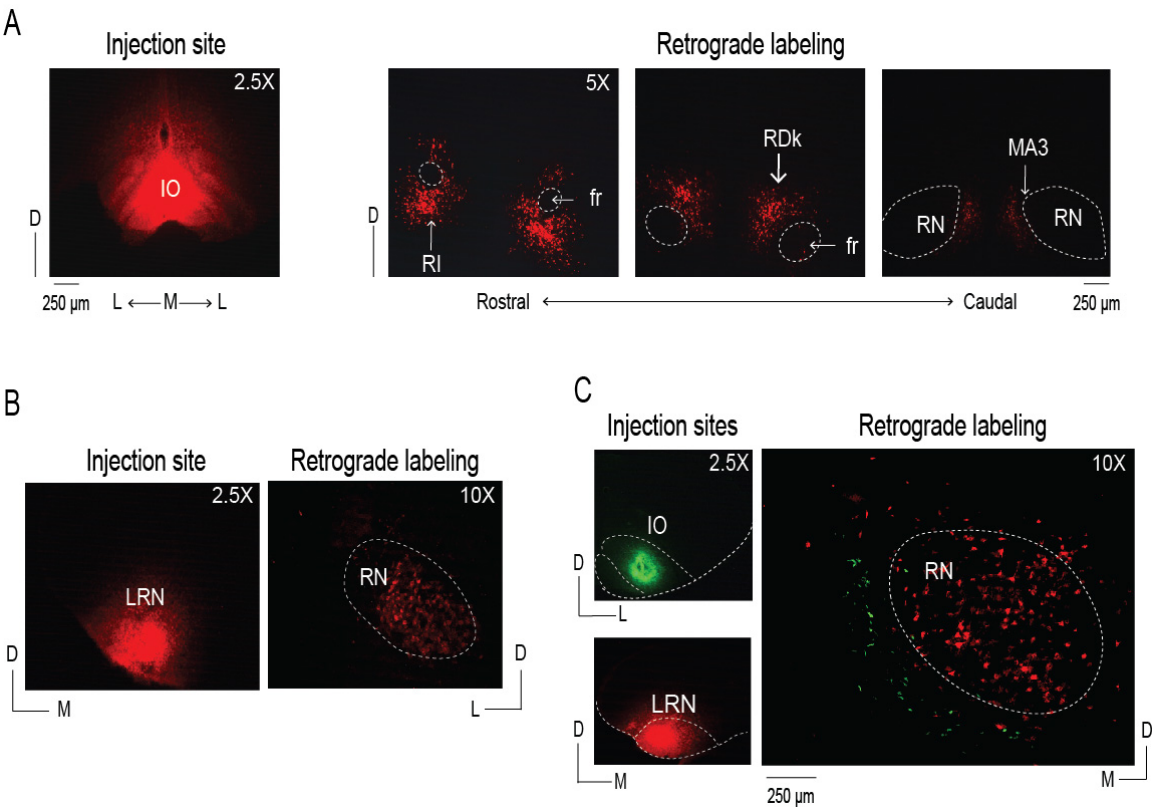

Fig 10. Retrograde labeling of the mesodiencephalic junction (MDJ) after infusion of WGA into the IO and LRN of P8 rats. (**A**) Left: Coronal section (2.5x) depicting WGA-555 diffusion in the IO. Right: Coronal sections (5x) depicting retrogradely labeled cell bodies in multiple MDJ nuclei. (**B**) Left: Coronal section (2.5x) depicting WGA-555 diffusion in the LRN. Right: Coronal section (10x) depicting retrogradely labeled cell bodies in the red nucleus (RN). (**C**) Left: Coronal sections (2.5x) depicting WGA-488 diffusion in the IO (top; green) and WGA-555 diffusion in the LRN (bottom; red) in the same P8 rat. Right: Coronal section (10x) depicting retrogradely labeled cell bodies in the RN (red; from LRN) and the region immediately medial to it (green; from RN). D: dorsal; L: lateral; M: medial; IO: inferior olive; RI: rostral interstitial nucleus of Cajal; fr: fasciculus retroflexus; RDk:

rostral nucleus of Darkschewitsch; MA3: accessory oculomotor nuclei; LRN: lateral reticular nucleus.

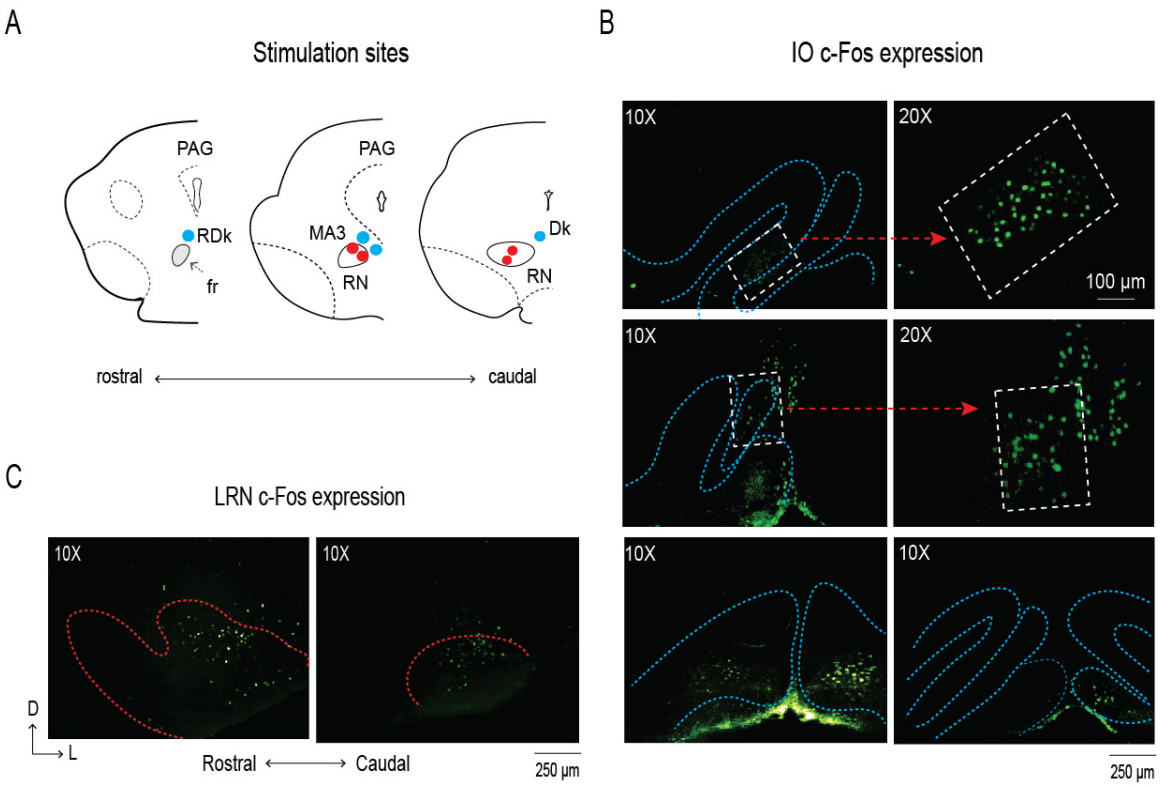

Fig 11. MDJ stimulation produces c-Fos expression in the IO and LRN. (**A**) Reconstruction of stimulation sites inside (red dots) and adjacent to (blue dots) the red nucleus (RN) in three coronal sections. (**B**) Representative photomicrographs in two different magnifications showing c-Fos expression in three sections of the IO (demarcated by blue dotted lines). (**C**) Representative photomicrographs showing c-Fos expression in two sections of the LRN (demarcated by red dotted lines). PAG: periaqueductal grey; RDk: rostral nucleus of Darkschewitsch; fr: fasciculus retroflexus; MA3: accessory oculomotor nucleus; Dk: nucleus Darkschewitsch; D=dorsal; L=lateral.

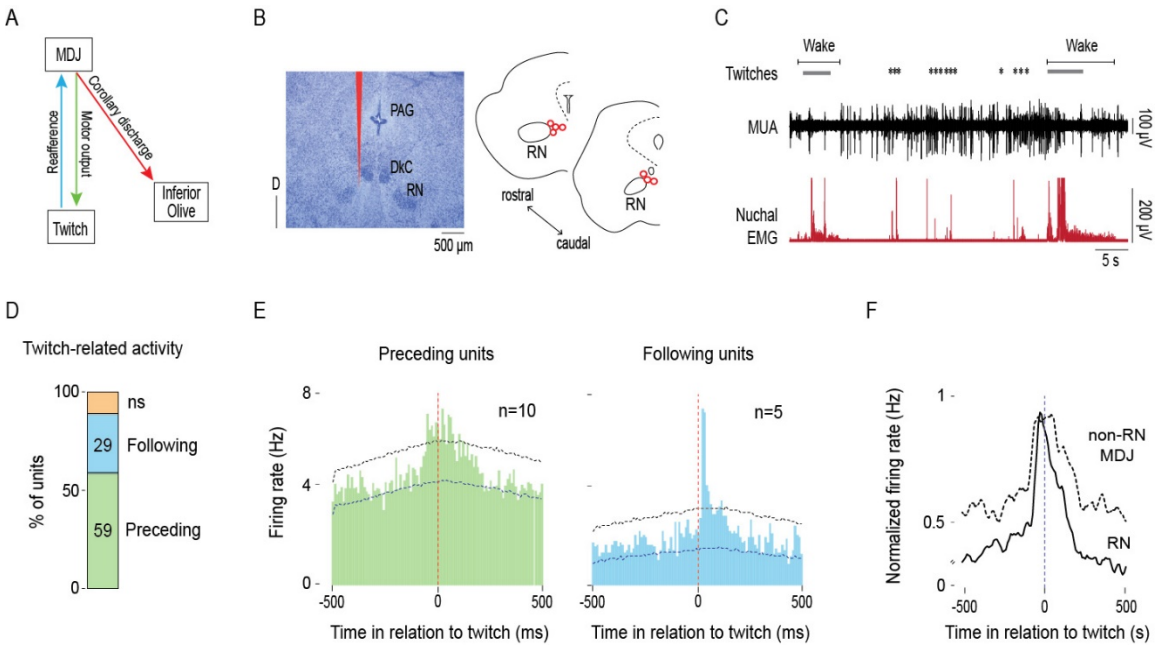

Fig 12. MDJ structures adjacent to the red nucleus exhibit twitch-preceding and twitch-following activity. (**A**) Diagram showing anatomical connections of the MDJ regions that lie adjacent to the red nucleus. Proposed pathways conveying motor commands (green line), reafference (blue line), and corollary discharge (red line) are shown. (**B**) Left: Reconstruction of a representative electrode placement (red vertical line; 2.5x). Right: Reconstruction of electrode placements (red circles) in the MDJ in two coronal sections across all pups (n=7). (**C**) Representative recording of rectified nuchal EMG activity and multiunit activity (MUA) in the MDJ during spontaneous sleep-wake cycling. Asterisks denote twitches and gray horizontal bars denote wake movements as scored by the experimenter. (**D**) Stacked plot depicting the percentage of twitch-preceding (motor; green) and twitch-following (sensory; blue) units in the MDJ. (**E**) Left: Perievent histogram (10-ms bins) showing cumulative activity of twitch-preceding MDJ units in relation to twitches. Data pooled across 10 units. Right: Perievent

histograms (10-ms bins) showing cumulative activity of twitch-following MDJ units in relation to twitches. Data pooled across 5 units. Red vertical dashed lines correspond to twitch onset. Upper and lower confidence bands ($p<0.05$ for each band) are indicated by black and blue horizontal dashed lines, respectively. (**F**) Perievent histograms (10-ms bins) comparing normalized firing rate in relation to twitch onset for twitch-preceding units in the red nucleus (RN; black solid line) with that of MDJ units adjacent to the red nucleus (black dashed line). The RN data are from a previously published study (Del Rio-Bermudez et al., 2015) and the MDJ data are from E, left. Black vertical dashed lines correspond to twitch onsets. D: dorsal; PAG: periaqueductal gray; DkC: caudal nucleus of Darkschewitsch; ns: not significant.

CHAPTER 4

Calcium-activated slow-potassium channels are responsible for the sharp peaks of olivary activity

Having identified motor structures that send CD to the IO and LRN, we next focused on understanding how a motor command with a broad twitch-preceding peak (see Fig 12F) is transformed into a sharp and precise CD peak around a twitch (see Fig 4C). We focused on the IO to address this question because of its reliably high percentage of units that exhibit twitch-related CD.

Excitatory presynaptic inputs to the IO result in an excitatory post-synaptic potential (EPSP), followed by an inhibitory post-synaptic potential (IPSP). The IPSP results in a long after-hyperpolarization in the IO (Mathy et al., 2009) that prevents temporal summation of excitatory presynaptic inputs (Garden et al., 2017). The inhibitory component is GABA-independent and is mediated by calcium-activated-slow potassium (SK) channels (Garden et al., 2017)

Because afferent projections from the MDJ to the IO are excitatory and because SK channels are expressed early in development in the rat IO (Gymnopoulos et al., 2014), we hypothesized that twitch-related CD from the MDJ results in the opening of SK channels in the IO, which truncates IO activity and results in sharp peaks. Accordingly, blocking SK channels should broaden the sharp CD peaks. To test this hypothesis, we blocked SK channels using apamin, an SK channel antagonist (Benington et al., 1995).

METHODS

Intra-olivary injection of apamin

In 18 P8 rats from 16 litters, pups were prepared for electrophysiological recording as described in CHAPTER 1, and transferred to the recording rig. Once a pup started cycling between sleep and wake, a 0.5 µl microsyringe was lowered stereotaxically into the IO and 100 nl of apamin. (Abcam, Cambridge, MA; 1 µM, dissolved in 0.9% saline, n=8) or saline (n=10) was injected over 1 min (Fig 13A). During preparation of the drug or vehicle, fluorogold (4%, Fluorochrome, Denver, CO) was added to the solutions for subsequent assessment of the extent of drug diffusion. After a 15-min period to allow for diffusion (the half-life of apamin is ~2 h; Gui et al., 2012), the microsyringe was withdrawn and a recording electrode was lowered in its place into the IO and activity was recorded for 30 min. At the end of the experiment, the pup was sacrificed and its brain was prepared for histology as described in CHAPTER 1.

Data analysis

First, we identified if apamin affected sleep-wake behavior. We assessed the amount of time spent in AS and the number of twitches per min of AS in each pup. Differences across groups were tested using the Mann-Whitney *U* test. Next, we determined if apamin altered the overall firing rate. We calculated the firing rate of each unit during AS and compared that across groups using the Mann-Whitney *U* test. One value exceeding 3 SD was excluded as an outlier.

We then assessed whether apamin altered the shape of twitch-triggered perievent histogram. First, we created perievent histograms (10-ms bins, 1-s window) for each unit as described above. For each unit, firing rate was normalized to the peak firing rate and the average normalized firing rate across all units in each group was calculated. Perievent histograms were then created with the average (+SEM) normalized firing rates triggered on twitches for each group. Next, we assessed how apamin altered the pattern of twitch-triggered activity of individual units. To do that, we identified significant units by performing jitter analysis on individual units as described in CHAPTER 1. We counted the percentage of units that showed precise peak within ±10 ms around a twitch and compared that across groups using a Chi-squared test. Finally, we pooled significant units in each group to create perievent histograms consisting of significant units only. To assess the difference in the shape of perievent histograms, we calculated the area under the curve within two particular time windows and compared that across groups using the Mann-Whitney *U* test. One value exceeding 3 SD was excluded as an outlier.

RESULTS

SK channels contribute to the sharp peak in olivary activity

We confirmed drug diffusion and recording sites within the IO (n=18 units across 10 pups in saline group; n= 21 units across 8 pups in apamin group; 1-3 units/pup; Fig 13B). There was no difference in the amount of time spent in AS or in the

number of twitches produced per unit time of AS between the apamin and saline groups (Fig 13C, left and middle). As observed in previous IO recordings, neural activity in both groups was phasic and restricted to periods of AS. There was no significant difference in the overall firing rate during AS between groups (Fig 13C, right).

Perievent histograms (1-s windows, 10-ms bins) were created across all units in each group (Fig 13D). Whereas twitch-triggered activity in the saline group exhibited the expected sharp peak around twitches, the activity in the apamin group exhibited a peak that was broader after twitches.

The number of units exhibiting significant twitch-related activity did not differ between the two groups (n=13/18 in saline and n=11/21 in apamin groups; X^2(1, N=39) = 1.6, p<0.3; Fig 13E). In contrast, the number of units exhibiting sharp peaks within ±10 ms of a twitch was significantly lower in the apamin group (5/21 units, 24%) than in the saline group (11/18 units, 61%; X^2(1, N=39) = 5.6, p<0.02; Fig 13E). To illustrate the effect of apamin on twitch-related activity, we pooled the data for the significant units to create perievent histograms of IO activity. As shown in Fig 13F, the activity in the apamin group, unlike that in saline group, persisted beyond the 10-ms window after a twitch. To quantify the difference, we calculated the area under the curve for each unit during two time windows: ±10 ms around a twitch and 20-200 ms after a twitch (Fig 13G). As expected, we found no significant difference between the two groups in the ±10-ms window (U=56.5, Z=-0.87, p<0.4), but did find a significant difference for the 20-200-ms window, with the apamin group being significantly larger (U=30.5, Z=-2.2, p<0.03). In fact, the

pattern of twitch-triggered neural activity in the apamin group was similar to that recorded in the MDJ (Figure 13H). These results suggest that SK channels are involved in sharpening of the CD signal arriving from the MDJ.

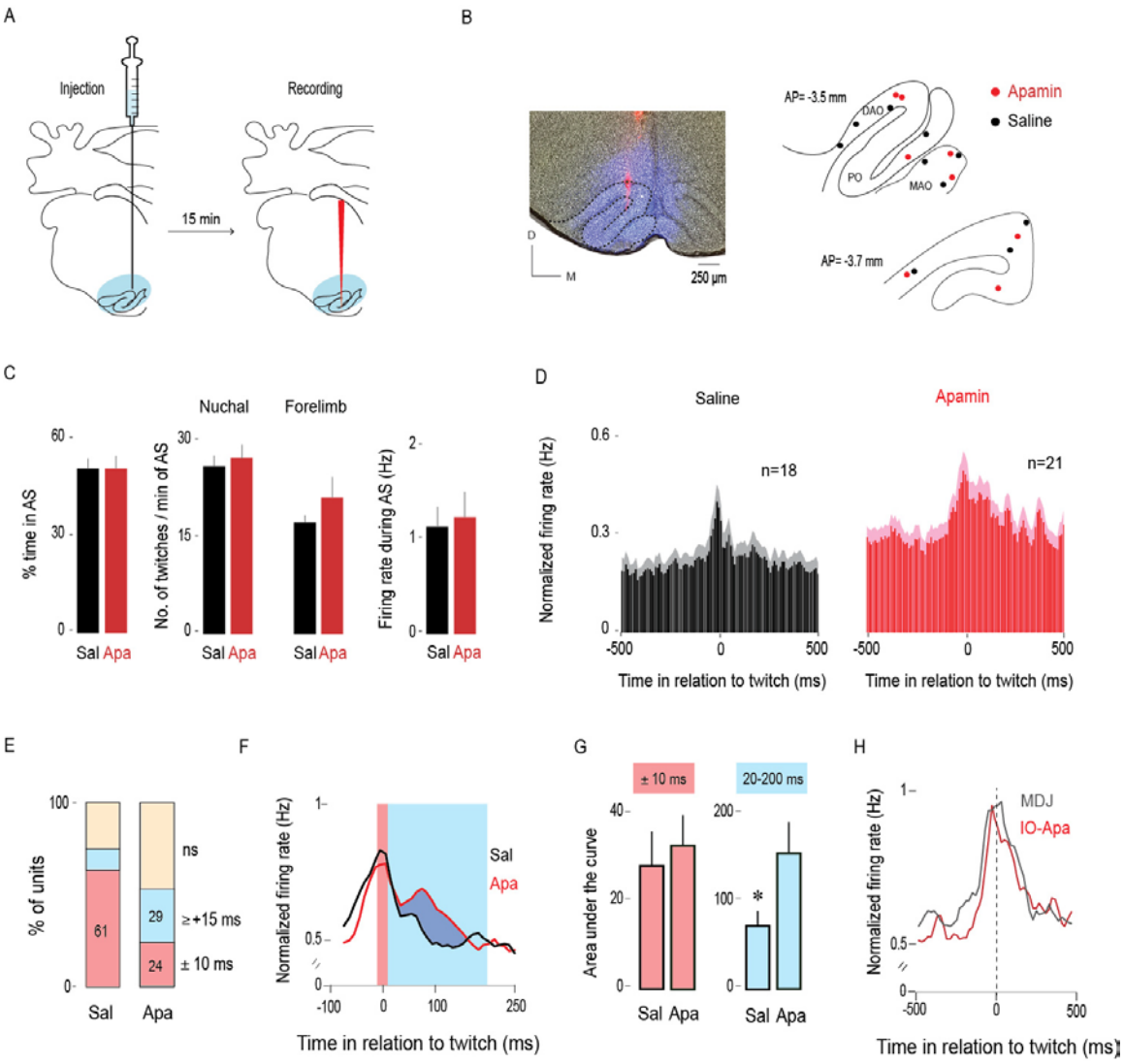

Fig 13. Apamin broadens the twitch-related peak in the IO. (**A**) Diagram depicting experimental design. Apamin or saline, mixed with 4% Fluorogold, was microinjected into the IO. Blue shaded area shows the extent of drug diffusion. Fifteen minutes after the injection, the microsyringe was withdrawn and a recording electrode, coated with DiI (red vertical line), was inserted into the IO. Unit activity was recorded for 30 min. (**B**) Left: Representative coronal section showing drug diffusion in the IO (blue shaded area) and placement of recording electrode (red) within the IO. Right: Reconstruction of electrode placements within the IO in two

coronal sections for all pups in the saline (black dots; n=10 pups) and apamin (red dots; n=8 pups) groups. (**C**) Bar graphs showing the mean (+SEM) percentage of time spent in AS (left), mean (+SEM) rates of nuchal and forelimb twitching per min of AS (middle; n=10 pups in saline and n=8 pups in apamin), and mean (+SEM) unit firing rates during AS (n=18 units in saline and n=23 units in apamin). (**D**) Perievent histograms (10-ms bins) showing mean (+SEM) normalized firing rate across all units triggered on twitches in the saline (n=18) and apamin (n=21) groups. (**E**) Stacked plots showing the percentage of units with significant activity within ±10 ms around twitches (red) and ≥15 ms following twitches (blue) in the saline and apamin groups. (**F**) Perievent histograms (10-ms bins) showing cumulative IO unit activity in relation to twitches in the saline (black line) and apamin (red line) groups. Data are pooled across significant units only (red + blue stacks in E) in both groups (n=13 in saline and n=11 in apamin group) and smoothed (tau=10 ms). Red shaded area denotes ±10-ms time window around twitches. Blue shaded area denotes 20-200-ms time window following twitches. (**G**) Bar graphs showing the area under the curve (mean + SEM) during two time windows; the ±10-ms window around twitches (red) and the 20-200-ms window following twitches (blue) for the units in the saline (n=12) and apamin (n=11) groups. * $p<0.03$. (**H**) Perievent histograms comparing normalized firing rate in relation to twitch onset for twitch-preceding units in the non-RN MDJ (gray line, taken from Figure 12E) with that of IO units in the apamin group (red line).DAO: dorsal accessory olive; MAO: medial accessory olive; PO: principal olive; D: dorsal;

M: medial; AP: antero-posterior in relation to bregma; sal: saline; apa: apamin; ns: not significant.

CHAPTER 5

Discussion and significance

We found that the IO and LRN of P8 rats exhibit twitch-related activity that cannot be categorized as either “motor” or “sensory.” The alternative is that this activity comprises a CD signal. If it is, then this would mean that twitches not only trigger reafference, but also produce a template against which that reafference can be compared—a form of self-monitoring that has not yet been demonstrated for this behavior.

In response to the accumulating evidence of CD in a diversity of species and systems, several criteria have been proposed (Poulet and Hedwig, 2007; Sommer and Wurtz, 2008). First, a CD signal should originate in a structure that is demonstrably involved in the production of movement; as shown here, the twitch-related signals in the IO and LRN originate from several independent premotor structures in the MDJ that are involved in the production of twitches and wake movements. A second criterion is that the areas receiving CD should themselves play no direct role in the production of movement, which is true of the IO and LRN (Gellman et al., 1985). A third criterion is that neurons receiving CD input should increase their activity at the onset of a movement; as shown here, the activity of IO and LRN neurons occurs precisely at the onset of twitches, exhibiting a temporal profile that clearly distinguishes it from twitch-preceding (motor) activity in the MDJ and twitch-following (sensory) activity in the ECN. Thus, we conclude that the twitch-related signals in the IO and LRN satisfy the key requirements of

CD. Below we discuss the characteristics of twitch-related CD and their implications and significance for sensorimotor development.

Neurophysiological identification of corollary discharge signals in behaving animals

Neural pathways conveying CD have been delineated in a diverse array of species (Davis et al., 1973; Fee et al., 1997; Sommer and Wurtz, 2002; Yang et al., 2008; Schneider et al., 2014; Dale and Cullen, 2017). Neural recordings of the CD signal itself, however, have mostly been performed in non-mammalian species; this includes the auditory system of crickets, the mechanosensory system of sea slugs, crayfish and tadpoles, and the electrosensory system of electric fish (Kirk and Wine, 1984; Evans et al., 2003; Li et al., 2004; Poulet and Hedwig, 2006; Requarth and Sawtell, 2014). The relatively small and simple nervous systems of these species have allowed researchers to isolate neurons that carry or receive CD signals and identify their relationship to motor behaviors.

In contrast, recordings of CD in mammals are rare. The first recording in a mammal was performed in the visuomotor system of primates (Sommer and Wurtz, 2004a). By recording from the mediodorsal thalamic nucleus (MD), it was shown that the activity in that structure precedes the onset of saccadic eye movements. Inactivation of the MD caused impairment of a movement-dependent task, which suggested that it receives CD from the superior colliculus (Sommer and Wurtz, 2004b).

Evidence of a CD signal has also been identified in the auditory cortex of mice, where sensory responses are suppressed during ongoing movements (Schneider et al., 2014). Recordings from interneurons in the auditory cortex revealed that the activity in those interneurons occurs before and during movements, and also precedes the suppression of cortical sensory neurons. The results suggested that those interneurons receive movement-related CD from the motor cortex.

The current findings add to this growing body of literature by providing the first direct neurophysiological evidence of CD in a developing mammal. Moreover, this is the first direct evidence of CD in the IO and LRN, structures that have been proposed to receive CD based on their connections with motor areas (De Zeeuw et al., 1998; Devor, 2002; Alstermark and Ekerot, 2013). More importantly, these findings reveal a unique neural signature for this twitch-related CD signal: the zero-latency peak and the sharp peak in activity. In addition, this signature provides a template to guide future neurophysiological investigations of CD signals in other species, brain structures, and sensory modalities across the lifespan.

A neural mechanism for sharpening the olivary corollary discharge signal

As mentioned above, one of the signature features of the twitch-related CD signal is the sharp peak. This is surprising because, as shown here and in a previous study (Del Rio-Bermudez et al., 2015), the twitch-preceding neurons within the MDJ exhibit broad peaks (see Fig 12F). How does a broad presynaptic signal in

the MDJ get converted into a sharp postsynaptic response in the IO and LRN (see Fig 4C, 8G)?

In cortical pyramidal neurons, interactions between excitatory and inhibitory inputs can sharpen a neuron's activity profile (Kremkow et al., 2010). In neurons that receive converging excitatory and inhibitory input, inhibition lags excitation by a few milliseconds, thereby creating a small window for temporal summation (Chance et al., 2002; Hasenstaub et al., 2005; Okun and Lampl, 2008; Rudolph et al., 2007). Inputs that fall outside the temporal window are not integrated by the postsynaptic neuron, thus effectively "sharpening" the post-synaptic response (Pouille and Scanziani, 2001). Here, to identify the inhibitory mechanism at work in the sharpening of CD responses around twitches, we focused on the IO because, compared with the LRN, a higher percentage of its units exhibited CD.

There are a few possible candidate mechanisms that could account for the sharp IO peaks. First, inhibitory interneurons in the IO could be activated by excitatory presynaptic inputs; however, interneurons are sparse in the IO (<0.1%, Nelson and Mugnaini, 1988), suggesting that this is an unlikely explanation. Alternatively, inhibitory feedback could arise from the deep cerebellar nuclei (DCN; de Zeeuw et al., 1988); however, activity in the DCN occurs ~40 ms after a twitch (Del Rio-Bermudez et al., 2016). Furthermore, in pilot experiments, pharmacological inactivation of the DCN did not have any effect on IO activity (data not shown).

Consequently, we hypothesized that inhibition in the IO is mediated by SK channels; in adult rats, these channels been shown to prevent summation of excitatory inputs in the IO (Garden et al., 2017). Using pharmacological inactivation at P8, we demonstrate that SK channels are indeed responsible for sharpening the olivary CD signal. A similar mechanism could be functional in the LRN as SK channels are also expressed in that structure in adult rats (Xu et al., 2013).

Learning to distinguish self from other

The developing sensorimotor system receives a substantial amount of sensory input primarily from two sources: self-generated twitches (reafference) and external stimulation (exafference). It has been suggested that the infant brain does not distinguish between these two sources of sensory input and that twitch-related reafference serves merely as a "proxy" for exafferent stimulation (Akhmetshina et al., 2016; McVea et al., 2016). This suggestion rests on the observation that both forms of stimulation, despite their very different origins, trigger similar patterns of cortical activity (Tiriac et al., 2012; Yang et al., 2013; Akhmetshina et al., 2016).

The current findings, however, suggest otherwise. Because CD accompanies the production of twitches, a mechanism is available to the infant brain for distinguishing the expected reafference arising from twitches from the unexpected exafferent stimuli arising from the outside world (e.g., mother and littermates). This finding introduces a new mechanism through which the developing nervous system can learn to distinguish between self-produced and other-produced movements (Blumberg and Dooley, 2017).

Differential actions of corollary discharge signals at precerebellar nuclei

The infant cerebellum receives a combination of CD and reafference from twitches via climbing fibers and mossy fibers (Sokoloff et al., 2015b; Sokoloff et al., 2015a). Here we provide direct evidence that twitch-related CD and reafference are processed distinctly in precerebellar nuclei before being conveyed to the cerebellum (Fig 14A).

In a previous study, it was demonstrated that the ECN processes reafference from twitches very differently from that of wake movements (Tiriac and Blumberg, 2016). Specifically, whereas twitch-related reafference was conveyed by the ECN to the cerebellum (via mossy fibers) and other downstream structures, wake-related reafference was gated within the ECN; when the ECN was pharmacologically disinhibited, wake-related reafference was unmasked. This finding indicated that the ECN is a neural comparator that is engaged in a state-dependent manner. A corollary of this finding is that CD signals (arriving directly or indirectly from the MDJ) act on the ECN to block wake-related reafference but that these signals are suspended or inhibited during twitching to allow the downstream conveyance of reafference.

In contrast with the ECN, the present findings demonstrate that twitch-related CD signals are received by the IO and LRN. These signals are not used to gate reafference, but rather are conveyed to the cerebellum (Fig 14A). In addition, like

the ECN, we found that the LRN receives twitch-related reafference from the periphery.

Within this broader context, we see that CD accompanies the production of twitches but its effects are not monolithic: It can modulate the action of a comparator to gate reafference (as in the ECN) or be transmitted sequentially to multiple downstream structures (as in the IO or LRN → cerebellum). Importantly, such differential effects of CD in different brain structures is also observed in adult animals. For example, in the vestibular nucleus of primates, CD is used to gate reafference from self-generated movements (Roy and Cullen, 2001); in the cerebellum-like structure of electric fish, CD helps to predict the sensory consequences of movements (Requarth and Sawtell, 2014). Our results are consistent with those observations and suggest that the same type of CD signal can exert different effects in different structures.

Altogether, our findings suggest that the precerebellar nuclei conspire to process and convey twitch-related information to the cerebellum. The common denominator of all this activity—both CD and reafference—is the inundation of the developing cerebellum with twitch-related information that, in turn, can facilitate activity-dependent development and sensorimotor integration in that structure (Fig 14A).

Wake-related suppression of precerebellar activity: possible underlying mechanisms

Whereas twitch-related reafference provides substantial input to the developing cerebellum, wake-related reafference does not (Sokoloff et al., 2015b; Sokoloff et al., 2015a). As demonstrated previously, at least some of this wake-related suppression occurs in the ECN (Tiriac and Blumberg, 2016). The current findings suggest that suppression also occurs in the IO and LRN (Figs 3D-F; 8C-E; 14B).

As shown in Figure 3D, a brief burst of IO activity often appeared at the onset of wake periods, followed quickly by its suppression. The LRN also exhibited brief activity at the onset of wake periods (see Fig 8C). In adults, movement-related suppression of activity is also observed in the IO and LRN. For example, in adult cats, activity is inhibited during voluntary movements in the IO (Rushmer et al., 1976; Gellman et al., 1985) and in a subpopulation of LRN neurons after the onset of scratching (Arshavsky et al., 1978). The present results in infant rats complement these earlier findings.

To account for wake-related suppression in the IO and LRN, it could be that these nuclei, like the ECN, act as neural comparators to gate wake-related reafference. For this to occur, individual neurons must receive converging CD and sensory input. Here, however, we found that IO neurons exhibiting CD-related activity were not responsive to reafference; and individual LRN neurons either exhibited CD-related activity or responsiveness to reafference, but not both. These findings are consistent with anatomical studies of the IO and LRN in adult rats

(Alstermark and Ekerot, 2013; De Zeeuw et al., 1998). Therefore, suppression of wake-related reafference in the IO and LRN is likely quite different from that occurring in the ECN.

In the IO, wake-related suppression could be mediated by serotonergic inputs that are known to exert inhibitory effects in the adult IO (Best and Regehr, 2008; Welsh et al., 1998). Because serotonin receptors are expressed in rats at P7 (Li et al., 2004), and because serotonergic structures projecting to the IO are active during wakefulness in rat pups (Karlsson et al., 2005), it is possible that serotonin released during wakefulness suppresses IO activity. Alternatively, activation of premotor structures at wake onset could suppress IO activity by activating inhibitory projection neurons that originate in the cuneate nucleus (Geborek et al., 2012). For the LRN, one possible mechanism is presynaptic inhibition within the spinal cord, where active suppression of sensory inputs is observed during voluntary movements in adult primates (Seki et al., 2003). The testing of these and other possible mechanisms remains for future experiments.

Functional implications of corollary discharge and reafference during development

Disruption of CD pathways has been shown to impair motor performances in adults (Sommer and Wurtz, 2004a). We did not attempt to demonstrate such impairments in this study, in part because pups at these ages do not appear to perform cerebellar-dependent motor tasks. However, we speculate that there are a number

of ways in which twitch-related CD could influence cerebellar development and function.

The adult cerebellum receives diverse inputs from self-generated movements (Proville et al., 2014). CD and reafference converge in the cerebellum via climbing and mossy fibers (van Kan et al., 1993; Wolpert et al., 1998; Huang et al., 2013), and it has been proposed that CD "predicts" the sensory consequences of an action (Marr, 1969; Albus, 1971; Blakemore et al., 2001). The comparison of "prediction" with "performance" is thought to be critical for sensorimotor integration and for the learning of complex motor behavior in adults (Marr, 1969; Albus, 1971; Manto et al., 2012; Proville et al., 2014).

Prediction of sensory consequences by CD, and its subsequent comparison with actual sensory feedback to compute prediction error, form the basis of the notion of forward models of motor learning (Blakemore et al., 2000). In adults, the cerebellum is thought to act as a forward model that receives sensory predictions and computes prediction errors from sensory feedback in order to facilitate motor learning (Wolpert et al., 1998; Blakemore et al., 2000; Requarth and Sawtell, 2014; Brooks et al., 2015).

To appreciate the potential significance of twitching for the developing cerebellum, consider this description of cerebellar function: "After much trial and error during infancy and throughout life, the cerebellum learns to associate actual movements with intended movements. Many of our motor memories are movements that we have repeated millions or billions of times..." (p. 538, Mason,

2011). In that context, the millions of twitches produced in early infancy could be a critical source of “practice” for the developing cerebellum. The convergence of twitch-related CD and reafference in that structure, as illustrated in Figure 14, would allow the cerebellum to compare “prediction” with “performance” and subsequently align prediction and feedback signals in a topographically organized fashion. Thus, by providing this converging input, twitches could contribute to the process by which forward models develop. Importantly, such models need to be updated throughout development as bodies and limbs develop and grow.

Finally, cerebellar circuitry undergoes substantial development over the first three postnatal weeks in rats (Altman, 1972b, a, c; Shimono et al., 1976; Wang and Zoghbi, 2001). Many of these developmental processes depend heavily on neural activity, including climbing fiber synapse elimination and translocation at Purkinje cells (Kakizawa et al., 2000; Andjus et al., 2003; Watanabe and Kano, 2011; Kano and Hashimoto, 2012). With respect to synapse elimination, beginning around P8, the initial multiple innervation of Purkinje cells by climbing fibers begins to shift toward singly innervated cells in the second postnatal week as one climbing fiber is selectively strengthened over others. Importantly, spike timing-dependent plasticity (STDP) has been implicated in this process (Kawamura et al., 2013); STDP depends on the repetitive and sequential firing of pre- and post-synaptic cells within a short and precise time window (Feldman, 2012; Kawamura et al., 2013; Sgritta et al., 2017). The present findings in precerebellar nuclei, in which twitch-related CD reliably preceded reafference by approximately 10-30 ms, are consistent with twitches playing a role in cerebellar development via STDP.

Moreover, recording from Purkinje cells at P8, we previously found that complex and simple spikes were highly likely to occur within 0-50 ms after twitches (Sokoloff et al., 2015b).

Implications for neurodevelopmental disorders

Sensorimotor dysfunction in early development could be responsible for later-emerging motor and cognitive deficits and mental illness. Therefore, a thorough understanding of sensorimotor processing during infancy, particularly during sleep, could be useful for early detection of atypical developmental trajectories.

Early cerebellar damage has been correlated with a number of neurodevelopmental disorders. For example, there is a well-established link between cerebellar dysfunction and autism spectrum disorder (ASD; Wang et al., 2014). It has been proposed that disruption of cerebellar function during sensitive periods of development—when "the cerebellum takes an early role in processing external sensory and internally generated information to influence neocortical circuit refinement" (p. 518; Wang et al., 2014)—could have negative cascading effects on cerebello-cortical communication and ultimately on associated cognitive processes, as observed in ASD.

Early cerebellar dysfunction can have genetic and non-genetic causes, including prenatal or postnatal exposure to environmental stressors. We propose that prolonged sleep deprivation or restriction could act as a potential environmental stressor during early postnatal development. As demonstrated in the current study and in previous studies (Sokoloff et al., 2015b; Sokoloff et al.,

2015a), AS provides an important context for cerebellar activity in early development. Therefore, perturbation of sleep could deprive the cerebellum of critical sensorimotor activity and thereby trigger downstream effects on cerebellar development. This could ultimately impact cerebello-cortical communications and result in cognitive impairment, as observed in ASD.

Accumulating evidence also suggests that CD-related processing is dysfunctional in patients with schizophrenia. Specifically, failure to disambiguate "self-generated" from "other-generated" sensory input may underlie hallucinations and delusions of control (Feinberg and Guazzelli, 1999; Ford et al., 2008). If twitches help to instruct the developing brain to distinguish self from other, disruption of sleep may have later-emerging negative consequences for the processing of CD. If so, then sensorimotor dysfunction during early development could be used as a biomarker for the emergence of neurological disorders later in life.

Conclusions

We conclude that twitches are accompanied by CD signals that are conveyed from premotor MDJ structures to the IO and LRN. In the IO and LRN, these signals trigger activity that exhibit unique signature features, including a sharp peak at the onset of a twitch. We also show that SK channels contribute to the sharpening of the CD peak.

It has been argued that the discreteness of twitches makes them ideally suited to provide high-fidelity sensory information at ages when activity-dependent

development is so important (Blumberg et al., 2013; Tiriac et al., 2015). The present results add to this notion by suggesting that convergence of twitch-related CD and reafference promotes sensorimotor integration during development. Convergence of twitch-related CD and reafferent inputs in the cerebellum not only provide the animal with continuously updated information about its developing body, but it also helps it distinguish between self- and other-generated movements. Altogether, converging input from millions of twitches provides ample opportunity for assimilating growing limbs into the developing nervous system, thereby enabling the infant to experience them as their own (Blumberg and Dooley, 2017).

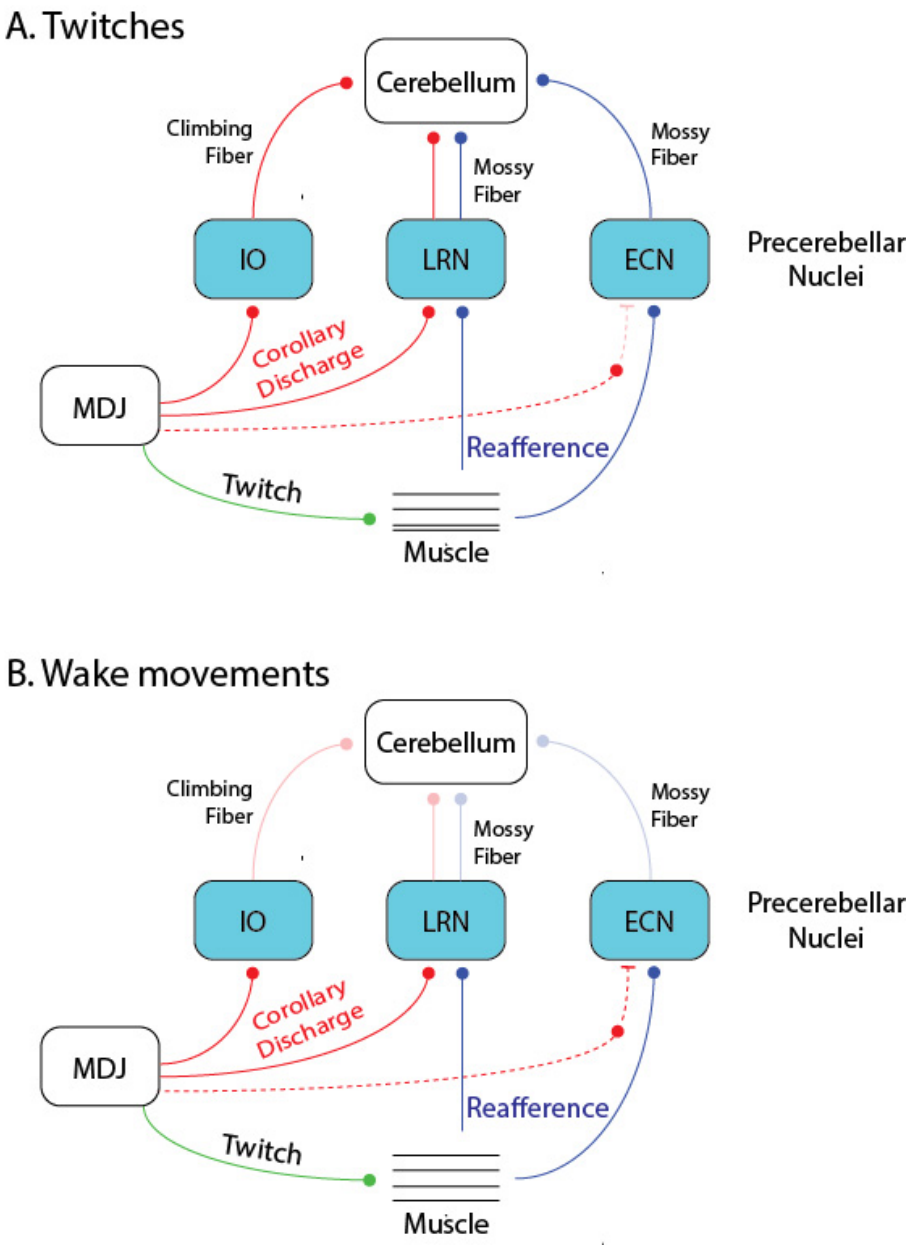

Fig 14. Schematic representation of pathways conveying information to the cerebellum in association with twitches and wake movements. (**A**) Flow of twitch-related CD from the MDJ to the IO and LRN and reafference from the limbs to the LRN and ECN. Both CD and reafference converge in the cerebellum via climbing and mossy fibers. Dotted lines denote hypothesized functional

connections. (**B**) Activity is suppressed during wake movements at all three precerebellar nuclei, thereby blocking input to the cerebellum.

REFERENCES

Akhmetshina D, Nasretdinov A, Zakharov A, Valeeva G, Khazipov R (2016) The nature of the sensory input to the neonatal rat barrel cortex. J Neurosci 36:9922-9932.

Albus JS (1971) A theory of cerebellar function. Mathematical Biosciences 10:25-61.

Alstermark B, Ekerot CF (2013) The lateral reticular nucleus: a precerebellar centre providing the cerebellum with overview and integration of motor functions at systems level. A new hypothesis. J Physiol 591:5453-5458.

Alstermark B, Ekerot CF (2015) The lateral reticular nucleus; integration of descending and ascending systems regulating voluntary forelimb movements. Front Comput Neurosci 9:102.

Altman J (1972a) Postnatal development of the cerebellar cortex in the rat. II. Phases in the maturation of Purkinje cells and of the molecular layer. J Comp Neurol 145:399-463.

Altman J (1972b) Postnatal development of the cerebellar cortex in the rat. I. The external germinal layer and the transitional molecular layer. J Comp Neurol 145:353-397.

Altman J (1972c) Postnatal development of the cerebellar cortex in the rat. 3. Maturation of the components of the granular layer. J Comp Neurol 145:465-513.

Amarasingham A, Harrison MT, Hatsopoulos NG, Geman S (2012) Conditional modeling and the jitter method of spike resampling. J Neurophysiol 107:517-531.

Andjus PR, Zhu L, Cesa R, Carulli D, Strata P (2003) A change in the pattern of activity affects the developmental regression of the Purkinje cell polyinnervation by climbing fibers in the rat cerebellum. Neuroscience 121:563-572.

Apps R (1999) Movement-related gating of climbing fibre input to cerebellar cortical zones. Prog Neurobiol 57:537-562.

Arshavsky YI, Gelfand IM, Orlovsky GN, Pavlova GA (1978) Messages conveyed by spinocerebellar pathways during scratching in the cat. I. Activity of neurons of the lateral reticular nucleus. Brain Res 151:479-491.

Azim E, Alstermark B (2015) Skilled forelimb movements and internal copy motor circuits. Curr Opin Neurobiol 33:16-24.

Azim E, Jiang J, Alstermark B, Jessell TM (2014) Skilled reaching relies on a V2a propriospinal internal copy circuit. Nature 508:357-363.

Benington JH, Woudenberg MC, Heller HC (1995) Apamin, a selective SK potassium channel blocker, suppresses REM sleep without a compensatory rebound. Brain Res 692:86-92.

Best AR, Regehr WG (2008) Serotonin evokes endocannabinoid release and retrogradely suppresses excitatory synapses. J Neurosci 28:6508-6515.

Blakemore SJ, Wolpert D, Frith C (2000) Why can't you tickle yourself? Neuroreport 11:R11-16.

Blakemore SJ, Frith CD, Wolpert DM (2001) The cerebellum is involved in predicting the sensory consequences of action. Neuroreport 12:1879-1884.
Blumberg MS (2010) Beyond dreams: do sleep-related movements contribute to brain development? Front Neurol 1:140.
Blumberg MS, Dooley JC (2017) Phantom limbs, neuroprosthetics, and the developmental origins of embodiment. Trends Neurosci 40:603-612.
Blumberg MS, Marques HG, Iida F (2013) Twitching in sensorimotor development from sleeping rats to robots. Curr Biol 23:R532-537.
Blumberg MS, Sokoloff G, Tiriac A, Del Rio-Bermudez C (2015) A valuable and promising method for recording brain activity in behaving newborn rodents. Dev Psychobiol 57:506-517.
Brooks JX, Carriot J, Cullen KE (2015) Learning to expect the unexpected: rapid updating in primate cerebellum during voluntary self-motion. Nat Neurosci 18:1310-1317.
Burroughs A, Wise AK, Xiao J, Houghton C, Tang T, Suh CY, Lang EJ, Apps R, Cerminara NL (2017) The dynamic relationship between cerebellar Purkinje cell simple spikes and the spikelet number of complex spikes. J Physiol 595:283-299.
Caputi AA (2004) Contributions of electric fish to the understanding of sensory processing by reafferent systems. J Physiol Paris 98:81-97.
Chung L (2015) A brief introduction to the transduction of neural activity into Fos signal. Dev Reprod 19:61-67.
Crapse TB, Sommer MA (2008) Corollary discharge across the animal kingdom. Nat Rev Neurosci 9:587-600.
Cullen KE (2004) Sensory signals during active versus passive movement. Curr Opin Neurobiol 14:698-706.
Dale A, Cullen KE (2017) The ventral posterior lateral thalamus preferentially encodes externally applied versus active movement: Implications for self-motion perception. Cereb Cortex:1-14.
Davis WJ, Siegler MV, Mpitoses (1973) Distributed neuronal oscillators and efference copy in the feeding system of Pleurobranchaea. J Neurophysiol 36:258-274.
de Zeeuw CI, Holstege JC, Calkoen F, Ruigrok TJ, Voogd J (1988) A new combination of WGA-HRP anterograde tracing and GABA immunocytochemistry applied to afferents of the cat inferior olive at the ultrastructural level. Brain Res 447:369-375.
De Zeeuw CI, Simpson JI, Hoogenraad CC, Galjart N, Koekkoek SK, Ruigrok TJ (1998) Microcircuitry and function of the inferior olive. Trends Neurosci 21:391-400.
Del Rio-Bermudez C, Sokoloff G, Blumberg MS (2015) Sensorimotor processing in the newborn rat red nucleus during active sleep. J Neurosci 35:8322-8332.
Del Rio-Bermudez C, Plumeau AM, Sattler NJ, Sokoloff G, Blumberg MS (2016) Spontaneous activity and functional connectivity in the developing cerebellorubral system. J Neurophysiol 116:1316-1327.

Desclin JC (1974) Histological evidence supporting the inferior olive as the major source of cerebellar climbing fibers in the rat. Brain Res 77:365-384.
Devor A (2002) The great gate: control of sensory information flow to the cerebellum. Cerebellum 1:27-34.
Eccles JC (1967) Circuits in the cerebellar control of movement. Proc Natl Acad Sci U S A 58:336-343.
Evans CG, Jing J, Proekt A, Rosen SC, Cropper EC (2003) Frequency-dependent regulation of afferent transmission in the feeding circuitry of Aplysia. J Neurophysiol 90:3967-3977.
Fee MS, Mitra PP, Kleinfeld D (1997) Central versus peripheral determinants of patterned spike activity in rat vibrissa cortex during whisking. J Neurophysiol 78:1144-1149.
Feinberg I, Guazzelli M (1999) Schizophrenia--a disorder of the corollary discharge systems that integrate the motor systems of thought with the sensory systems of consciousness. Br J Psychiatry 174:196-204.
Feldman DE (2012) The spike-timing dependence of plasticity. Neuron 75:556-571.
Ford JM, Roach BJ, Faustman WO, Mathalon DH (2008) Out-of-synch and out-of-sorts: dysfunction of motor-sensory communication in schizophrenia. Biol Psychiatry 63:736-743.
Fukushima K (1991) The interstitial nucleus of Cajal in the midbrain reticular formation and vertical eye movement. Neurosci Res 10:159-187.
Garden DL, Rinaldi A, Nolan MF (2017) Active integration of glutamatergic input to the inferior olive generates bidirectional postsynaptic potentials. J Physiol 595:1239-1251.
Gassel MM, Marchiafava PL, Pompeiano O (1964) Phasic Changes in Muscular Activity during Desynchronized Sleep in Unrestrained Cats. An Analysis of the Pattern and Organization of Myoclonic Twitches. Arch Ital Biol 102:449-470.
Geborek P, Jorntell H, Bengtsson F (2012) Stimulation within the cuneate nucleus suppresses synaptic activation of climbing fibers. Front Neural Circuits 6:120.
Gellman R, Houk JC, Gibson AR (1983) Somatosensory properties of the inferior olive of the cat. J Comp Neurol 215:228-243.
Gellman R, Gibson AR, Houk JC (1985) Inferior olivary neurons in the awake cat: detection of contact and passive body displacement. J Neurophysiol 54:40-60.
Gramsbergen A, Schwartze P, Prechtl HF (1970) The postnatal development of behavioral states in the rat. Dev Psychobiol 3:267-280.
Gui L, LaGrange LP, Larson RA, Gu M, Zhu J, Chen QH (2012) Role of small conductance calcium-activated potassium channels expressed in PVN in regulating sympathetic nerve activity and arterial blood pressure in rats. Am J Physiol Regul Integr Comp Physiol 303:R301-310.
Gymnopoulos M, Cingolani LA, Pedarzani P, Stocker M (2014) Developmental mapping of small-conductance calcium-activated potassium channel expression in the rat nervous system. J Comp Neurol 522:1072-1101.

Harrison MT, Geman S (2009) A rate and history-preserving resampling algorithm for neural spike trains. Neural Comput 21:1244-1258.
Hasenstaub A, Shu Y, Haider B, Kraushaar U, Duque A, McCormick DA (2005) Inhibitory postsynaptic potentials carry synchronized frequency information in active cortical networks. Neuron 47:423-435.
Hausser M, Clark BA (1997) Tonic synaptic inhibition modulates neuronal output pattern and spatiotemporal synaptic integration. Neuron 19:665-678.
Holst EV, Mittelstaedt H (1950) The reafference principle. Naturwissenschaften 37:464-467.
Huang CC, Sugino K, Shima Y, Guo C, Bai S, Mensh BD, Nelson SB, Hantman AW (2013) Convergence of pontine and proprioceptive streams onto multimodal cerebellar granule cells. Elife 2:e00400.
Inacio AR, Nasretdinov A, Lebedeva J, Khazipov R (2016) Sensory feedback synchronizes motor and sensory neuronal networks in the neonatal rat spinal cord. Nat Commun 7:13060.
Jouvet-Mounier D, Astic L, Lacote D (1970) Ontogenesis of the states of sleep in rat, cat, and guinea pig during the first postnatal month. Dev Psychobiol 2:216-239.
Kakizawa S, Yamasaki M, Watanabe M, Kano M (2000) Critical period for activity-dependent synapse elimination in developing cerebellum. J Neurosci 20:4954-4961.
Kano M, Hashimoto K (2012) Activity-dependent maturation of climbing fiber to Purkinje cell synapses during postnatal cerebellar development. Cerebellum 11:449-450.
Karlsson KA, Gall AJ, Mohns EJ, Seelke AM, Blumberg MS (2005) The neural substrates of infant sleep in rats. PLoS Biol 3:e143.
Kawamura Y, Nakayama H, Hashimoto K, Sakimura K, Kitamura K, Kano M (2013) Spike timing-dependent selective strengthening of single climbing fibre inputs to Purkinje cells during cerebellar development. Nat Commun 4:2732.
Khazipov R, Sirota A, Leinekugel X, Holmes GL, Ben-Ari Y, Buzsaki G (2004) Early motor activity drives spindle bursts in the developing somatosensory cortex. Nature 432:758-761.
Kirk MD, Wine JJ (1984) Identified interneurons produce both primary afferent depolarization and presynaptic inhibition. Science 225:854-856.
Krasne FB, Bryan JS (1973) Habituation: regulation through presynaptic inhibition. Science 182:590-592.
Kreider JC, Blumberg MS (2000) Mesopontine contribution to the expression of active 'twitch' sleep in decerebrate week-old rats. Brain Res 872:149-159.
Kremkow J, Perrinet LU, Masson GS, Aertsen A (2010) Functional consequences of correlated excitatory and inhibitory conductances in cortical networks. J Comput Neurosci 28:579-594.
Lakke EA (1997) The projections to the spinal cord of the rat during development: a timetable of descent. Adv Anat Embryol Cell Biol 135:I-XIV, 1-143.

Lee HS, Mihailoff GA (1990) Convergence of cortical and cerebellar projections on single basilar pontine neurons: a light and electron microscopic study in the rat. Neuroscience 39:561-577.
Li WC, Higashijima S, Parry DM, Roberts A, Soffe SR (2004) Primitive roles for inhibitory interneurons in developing frog spinal cord. J Neurosci 24:5840-5848.
Manto M, Bower JM, Conforto AB, Delgado-Garcia JM, da Guarda SN, Gerwig M, Habas C, Hagura N, Ivry RB, Marien P, Molinari M, Naito E, Nowak DA, Oulad Ben Taib N, Pelisson D, Tesche CD, Tilikete C, Timmann D (2012) Consensus paper: roles of the cerebellum in motor control--the diversity of ideas on cerebellar involvement in movement. Cerebellum 11:457-487.
Marcano-Reik AJ, Prasad T, Weiner JA, Blumberg MS (2010) An abrupt developmental shift in callosal modulation of sleep-related spindle bursts coincides with the emergence of excitatory-inhibitory balance and a reduction of somatosensory cortical plasticity. Behav Neurosci 124:600-611.
Marr D (1969) A theory of cerebellar cortex. J Physiol 202:437-470.
Mason P (2011) Medical Neurobiology. New York: Oxford University Press.
Mathy A, Ho SS, Davie JT, Duguid IC, Clark BA, Hausser M (2009) Encoding of oscillations by axonal bursts in inferior olive neurons. Neuron 62:388-399.
McVea DA, Murphy TH, Mohajerani MH (2016) Large scale cortical functional networks associated with slow-wave and spindle-burst-related spontaneous activity. Front Neural Circuits 10:103.
Milh M, Kaminska A, Huon C, Lapillonne A, Ben-Ari Y, Khazipov R (2007) Rapid cortical oscillations and early motor activity in premature human neonate. Cereb Cortex 17:1582-1594.
Mohns EJ, Blumberg MS (2010) Neocortical activation of the hippocampus during sleep in infant rats. J Neurosci 30:3438-3449.
Morris R, Vallester KK, Newton SS, Kearsley AP, Whishaw IQ (2015) The differential contributions of the parvocellular and the magnocellular subdivisions of the red nucleus to skilled reaching in the rat. Neuroscience 295:48-57.
Mukherjee D, Yonk AJ, Sokoloff G, Blumberg MS (2017) Wakefulness suppresses retinal wave-related neural activity in visual cortex. J Neurophysiol 118:1190-1197.
Nelson BJ, Mugnaini E (1988) The rat inferior olive as seen with immunostaining for glutamate decarboxylase. Anat Embryol (Berl) 179:109-127.
Neuweiler G (2003) Evolutionary aspects of bat echolocation. J Comp Physiol A Neuroethol Sens Neural Behav Physiol 189:245-256.
Okun M, Lampl I (2008) Instantaneous correlation of excitation and inhibition during ongoing and sensory-evoked activities. Nat Neurosci 11:535-537.
Onodera S, Hicks TP (1996) A projection linking motor cortex with the LM-suprageniculate nuclear complex through the periaqueductal gray area which surrounds the nucleus of Darkschewitsch in the cat. Prog Brain Res 112:85-98.

Onodera S, Hicks TP (2009) A comparative neuroanatomical study of the red nucleus of the cat, macaque and human. PLoS One 4:e6623.
Petersson P, Waldenstrom A, Fahraeus C, Schouenborg J (2003) Spontaneous muscle twitches during sleep guide spinal self-organization. Nature 424:72-75.
Pivetta C, Esposito MS, Sigrist M, Arber S (2014) Motor-circuit communication matrix from spinal cord to brainstem neurons revealed by developmental origin. Cell 156:537-548.
Pouille F, Scanziani M (2001) Enforcement of temporal fidelity in pyramidal cells by somatic feed-forward inhibition. Science 293:1159-1163.
Poulet JF, Hedwig B (2006) The cellular basis of a corollary discharge. Science 311:518-522.
Poulet JF, Hedwig B (2007) New insights into corollary discharges mediated by identified neural pathways. Trends Neurosci 30:14-21.
Proville RD, Spolidoro M, Guyon N, Dugue GP, Selimi F, Isope P, Popa D, Lena C (2014) Cerebellum involvement in cortical sensorimotor circuits for the control of voluntary movements. Nat Neurosci 17:1233-1239.
Puro DG, Woodward DJ (1977) Maturation of evoked climbing fiber input to rat cerebellar purkinje cells (I.). Exp Brain Res 28:85-100.
Reeber SL, White JJ, George-Jones NA, Sillitoe RV (2012) Architecture and development of olivocerebellar circuit topography. Front Neural Circuits 6:115.
Requarth T, Sawtell NB (2014) Plastic corollary discharge predicts sensory consequences of movements in a cerebellum-like circuit. Neuron 82:896-907.
Robinson SR, Kleven GA, Brumley MR (2008) Prenatal Development of Interlimb Motor Learning in the Rat Fetus. Infancy 13:204-228.
Robinson SR, Blumberg MS, Lane MS, Kreber LA (2000) Spontaneous motor activity in fetal and infant rats is organized into discrete multilimb bouts. Behav Neurosci 114:328-336.
Roffwarg HP, Muzio JN, Dement WC (1966) Ontogenetic development of the human sleep-dream cycle. Science 152:604-619.
Roy JE, Cullen KE (2001) Selective processing of vestibular reafference during self-generated head motion. J Neurosci 21:2131-2142.
Ruigrok TJ, Voogd J (2000) Organization of projections from the inferior olive to the cerebellar nuclei in the rat. J Comp Neurol 426:209-228.
Ruigrok TJ, Sillitoe RV, Voogd J (2014) Cerebellum and cerebellar connections In: The Rat Nervous System, 4 Edition (Paxinos G, ed), pp 133-204. UK: Elsevier Academic Press.
Rushmer DS, Roberts WJ, Augter GK (1976) Climbing fiber responses of cerebellar Purkinje cells to passive movement of the cat forepaw. Brain Res 106:1-20.
Saint-Cyr JA (1983) The projection from the motor cortex to the inferior olive in the cat. An experimental study using axonal transport techniques. Neuroscience 10:667-684.

Saint-Cyr JA, Courville J (1981) Sources of descending afferents to the inferior olive from the upper brain stem in the cat as revealed by the retrograde transport of horseradish peroxidase. J Comp Neurol 198:567-581.
Schneider DM, Nelson A, Mooney R (2014) A synaptic and circuit basis for corollary discharge in the auditory cortex. Nature 513:189-194.
Sedgwick EM, Williams TD (1967) Responses of single units in the inferior olive to stimulation of the limb nerves, peripheral skin receptors, cerebellum, caudate nucleus and motor cortex. J Physiol 189:261-279.
Seelke AMH, Blumberg MS (2008) The microstructure of active and quiet sleep as cortical delta activity emerges in infant rats. Sleep 31:691-699.
Seelke AMH, Blumberg MS (2010) The form and function of infant sleep: From muscle to neocortex. In: The Oxford Handbook of Developmental Behavioral Neuroscience (Blumberg MS, Freeman JH, Robinson SR, eds), pp 391-423. New York: Oxford University Press.
Seki K, Perlmutter SI, Fetz EE (2003) Sensory input to primate spinal cord is presynaptically inhibited during voluntary movement. Nat Neurosci 6:1309-1316.
Sgritta M, Locatelli F, Soda T, Prestori F, D'Angelo EU (2017) Hebbian Spike-Timing Dependent Plasticity at the Cerebellar Input Stage. J Neurosci 37:2809-2823.
Shimono T, Nosaka S, Sasaki K (1976) Electrophysiological study on the postnatal development of neuronal mechanisms in the rat cerebellar cortex. Brain Res 108:279-294.
Sokoloff G, Uitermarkt BD, Blumberg MS (2015a) REM sleep twitches rouse nascent cerebellar circuits: Implications for sensorimotor development. Dev Neurobiol 75:1140-1153.
Sokoloff G, Plumeau AM, Mukherjee D, Blumberg MS (2015b) Twitch-related and rhythmic activation of the developing cerebellar cortex. J Neurophysiol 114:1746-1756.
Sommer MA, Wurtz RH (2002) A pathway in primate brain for internal monitoring of movements. Science 296:1480-1482.
Sommer MA, Wurtz RH (2004a) What the brain stem tells the frontal cortex. I. Oculomotor signals sent from superior colliculus to frontal eye field via mediodorsal thalamus. J Neurophysiol 91:1381-1402.
Sommer MA, Wurtz RH (2004b) What the brain stem tells the frontal cortex. II. Role of the SC-MD-FEF pathway in corollary discharge. J Neurophysiol 91:1403-1423.
Sommer MA, Wurtz RH (2008) Brain circuits for the internal monitoring of movements. Annu Rev Neurosci 31:317-338.
Sperry RW (1950) Neural basis of the spontaneous optokinetic response produced by visual inversion. J Comp Physiol Psychol 43:482-489.
Stefani A, Gabelia D, Mitterling T, Poewe W, Hogl B, Frauscher B (2015) A Prospective Video-Polysomnographic Analysis of Movements during Physiological Sleep in 100 Healthy Sleepers. Sleep 38:1479-1487.

Sugihara I, Wu HS, Shinoda Y (2001) The entire trajectories of single olivocerebellar axons in the cerebellar cortex and their contribution to Cerebellar compartmentalization. J Neurosci 21:7715-7723.
Tiriac A, Blumberg MS (2016) Gating of reafference in the external cuneate nucleus during self-generated movements in wake but not sleep. Elife 5.
Tiriac A, Del Rio-Bermudez C, Blumberg MS (2014) Self-generated movements with "unexpected" sensory consequences. Curr Biol 24:2136-2141.
Tiriac A, Sokoloff G, Blumberg MS (2015) Myoclonic Twitching and Sleep-Dependent Plasticity in the Developing Sensorimotor System. Curr Sleep Med Rep 1:74-79.
Tiriac A, Uitermarkt BD, Fanning AS, Sokoloff G, Blumberg MS (2012) Rapid whisker movements in sleeping newborn rats. Curr Biol 22:2075-2080.
van Kan PL, Gibson AR, Houk JC (1993) Movement-related inputs to intermediate cerebellum of the monkey. J Neurophysiol 69:74-94.
Wang SS, Kloth AD, Badura A (2014) The cerebellum, sensitive periods, and autism. Neuron 83:518-532.
Wang VY, Zoghbi HY (2001) Genetic regulation of cerebellar development. Nat Rev Neurosci 2:484-491.
Watanabe M, Kano M (2011) Climbing fiber synapse elimination in cerebellar Purkinje cells. Eur J Neurosci 34:1697-1710.
Welsh JP, Chang B, Menaker ME, Aicher SA (1998) Removal of the inferior olive abolishes myoclonic seizures associated with a loss of olivary serotonin. Neuroscience 82:879-897.
Williams PT, Kim S, Martin JH (2014) Postnatal maturation of the red nucleus motor map depends on rubrospinal connections with forelimb motor pools. J Neurosci 34:4432-4441.
Wolpert DM, Miall RC, Kawato M (1998) Internal models in the cerebellum. Trends Cogn Sci 2:338-347.
Xu W, Jones S, Edgley SA (2013) Event time representation in cerebellar mossy fibres arising from the lateral reticular nucleus. J Physiol 591:1045-1062.
Yang JW, An S, Sun JJ, Reyes-Puerta V, Kindler J, Berger T, Kilb W, Luhmann HJ (2013) Thalamic network oscillations synchronize ontogenetic columns in the newborn rat barrel cortex. Cereb Cortex 23:1299-1316.
Yang Y, Cao P, Yang Y, Wang SR (2008) Corollary discharge circuits for saccadic modulation of the pigeon visual system. Nat Neurosci 11:595-602.
Zuk A, Rutherford JG, Gwyn DG (1983) Projections from the interstitial nucleus of Cajal to the inferior olive and to the spinal cord in cat: a retrograde fluorescent double-labeling study. Neurosci Lett 38:95-101.